Global Biogeochemical Cycles

RESEARCH ARTICLE
10.1029/2020GB006599

Key Points:
- We use publicly available nitrate and inorganic carbon data from profiling floats to solve tracer budgets for net community production
- Our estimates of seasonal and annual net community production agree well with previously published results
- Using multiple budgets, we are able to differentiate the dissolved and particulate organic, and particulate inorganic, carbon export pools

Supporting Information:
- Supporting Information S1

Correspondence to:
A. J. Fassbender,
fassbender@mbari.org

Citation:
Haskell, W. Z. II, Fassbender, A. J., Long, J. S., & Plant, J. N. (2020). Annual net community production of particulate and dissolved organic carbon from a decade of biogeochemical profiling float observations in the Northeast Pacific. *Global Biogeochemical Cycles*, *34*, e2020GB006599. https://doi.org/10.1029/2020GB006599

Received 12 MAR 2020
Accepted 4 OCT 2020
Accepted article online 13 OCT 2020

Annual Net Community Production of Particulate and Dissolved Organic Carbon From a Decade of Biogeochemical Profiling Float Observations in the Northeast Pacific

W. Z. Haskell II[1], A. J. Fassbender[1], J. S. Long[1], and J. N. Plant[1]

[1]Monterey Bay Aquarium Research Institute, Moss Landing, CA, USA

Abstract Carbon export out of the surface ocean via the biological pump is a critical sink for atmospheric carbon dioxide. This process transports organic carbon to the deep ocean through sinking particulate organic carbon (POC) and the downward transport of suspended POC and dissolved organic carbon (DOC). Changes in the relative contribution of each pathway can significantly affect the magnitude and efficiency of carbon export to depth. Net community production (NCP), an analog of carbon export under steady state assumptions, is typically estimated using budgets of biologically important chemical tracers in the upper ocean constrained by ship-board or autonomous platform observations. In this study, we use measurements from biogeochemical profiling floats, the Ocean Station Papa mooring, and recently developed algorithms for carbonate system parameters to constrain budgets for three tracers (nitrate, dissolved inorganic carbon, and total alkalinity) and estimate NCP in the Northeast Pacific from 2009 to 2017. Using our multiple-tracer approach, and constraining end-member nutrient ratios of the POC and DOC produced, we not only calculate regional NCP throughout the annual cycle and across multiple depth horizons, but also partition this quantity into particulate and dissolved portions. We also use a particle backscatter-based approach to estimate POC attenuation with depth and present a new method to constrain particle export across deeper horizons and estimate in situ export efficiency. Our results agree well with previously published estimates of regional carbon export annually and suggest that the approaches presented here could be used to assess the magnitude and efficiency of carbon export in other regions of the world's oceans.

Plain Language Summary "Carbon export" refers to the amount of carbon dioxide that is removed from the atmosphere by organisms in the surface ocean and subsequently transported into the deep sea, either through sinking particles (more efficient process) or downward mixing (less efficient process), making the ocean a natural sink for atmospheric carbon dioxide and significantly influencing ocean chemistry. The relative proportion of export through each pathway significantly affects the overall efficiency of this process and has implications for the pattern of carbon export globally. Measuring carbon export throughout the year traditionally requires persistent ship-based observations, which can be costly and perilous for researchers. Instead, carbon export is often estimated by budgeting nutrient distributions and changes through time, as they are also controlled by the same processes. These measurements can now be made remotely using autonomous biogeochemical profiling floats. Here, we present a new approach utilizing multiple chemical budgets to estimate carbon export over a decade in the Northeast Pacific, which can be combined to partition export occurring through sinking particles and downward mixing. Our results are supported by previously published estimates of carbon export and suggest that this method has the potential to be applied to other parts of the ocean.

1. Introduction

By reducing the partial pressure of carbon dioxide gas (pCO_2) in the surface ocean that is in equilibrium with the atmosphere, organic carbon export via the biological pump (Volk & Hoffert, 1985) is central to maintaining the vertical gradient in dissolved inorganic carbon (DIC) in the oceans and thus the oceanic sink for atmospheric carbon dioxide (Sarmiento & Siegenthaler, 1992). Although carbon export can occur through many pathways (i.e., particle injection pumps [PIPs], Boyd et al., 2019; seasonal mixed layer pump, Dall'Olmo et al., 2016; eddy subduction of waters with high carbon concentration, Omand et al., 2015;

and zooplankton vertical migration, Steinberg et al., 2000), the relative contribution of the gravitational sinking of particulate organic carbon (POC) and downward mixing of dissolved organic carbon (DOC) is important in determining the magnitude and efficiency of carbon export globally (Hansell et al., 2009; Lomas & Bates, 2004; Martin et al., 1987). For example, particles typically sink faster than the rate of downward mixing of DOC. Furthermore, the ultimate fate of the products of primary production is influenced by this partitioning of organic carbon (fueling the mesopelagic macrobial vs. microbial food webs, De La Rocha & Passow, 2014; del Giorgio & Duarte, 2002). However, measuring the evolution of each quantity over seasons to years is particularly difficult because it traditionally requires persistent ship-based observations (Hansell & Carlson, 2001; Owens et al., 2013), including during hostile winter conditions. Thus, a scalable, remotely monitored, autonomous sampling approach is desirable.

Net community production (NCP) is the difference between gross primary production and total respiration and is equivalent to the amount of carbon fixed during primary production (both POC and DOC) that is available for export out of the surface ocean at steady state when integrated over sufficiently long time and space scales (Brix et al., 2006; Emerson, 1987). Typically, NCP is estimated using budgets of chemical tracers in the surface ocean (Emerson, 2014), many of which can be measured using sensors on autonomous platforms (Nicholson et al., 2008; Riser & Johnson, 2008). Biogeochemical (BGC) profiling floats, in particular, provide a means of persistent observation for multiple annual cycles without the need for continued maintenance and, because of this, have been increasingly used for carbon export studies (Bushinsky & Emerson, 2018; Johnson et al., 2017; Llort et al., 2018; Williams et al., 2018; Yang et al., 2017).

In the Northeast Pacific, a region of high atmospheric carbon dioxide gas (CO_2) uptake (Ayers & Lozier, 2012; Takahashi et al., 2009), NCP has been estimated using sensor measurements from floats and gliders (Bushinsky & Emerson, 2015; Emerson & Stump, 2010; Emerson et al., 2008; Nicholson et al., 2008; Pelland et al., 2018; Plant et al., 2016) as well as the National Oceanic and Atmospheric Administration (NOAA) Station Papa mooring, where Fassbender et al. (2016) applied dual tracer budgets (DIC and total alkalinity [TA]) to calculate NCP and the production of calcium carbonate ($CaCO_3$), a known ballast material for sinking particles (Armstrong et al., 2002). Theoretically, if POC and DOC produced through NCP have distinct nutrient stoichiometries (Letscher et al., 2015), NCP can also be partitioned into the contributions from particulate and dissolved organic pools when the carbon begins its downward journey into the abyss.

Here, we use measurements from autonomous BGC profiling floats (nitrate [NO_3^-] and oxygen [O_2]), the Station Papa mooring (pCO_2), and recently developed algorithms for carbonate system parameters (DIC and TA) (Bittig et al., 2018; Carter et al., 2017) to build one-dimensional budgets of three biogeochemical tracers (DIC, TA, and NO_3^-) in the Northeast Pacific from 2009 through 2017. Our goals are to (1) calculate the rates of biweekly to annual NCP (ANCP) and $CaCO_3$ production over the last decade and across multiple relevant depth zones (similar to the approaches of Fassbender et al., 2016, and Plant et al., 2016); (2) constrain transport rates (eddy diffusivity, gas exchange, entrainment velocity, etc.) and nutrient ratios in the region during community production in the surface ocean and remineralization at depth; (3) partition budget-based NCP into POC and DOC production using constraints on the C:N ratio of each carbon pool; and (4) use particle backscatter measurements to estimate the attenuation of sinking particles with depth and calculate particle export across deeper horizons.

These production estimates are designed to support the efforts of the ongoing National Aeronautics and Space Administration (NASA) Export Processes in the Ocean from Remote Sensing (EXPORTS) program by providing carbon export estimates over multiple timescales from in situ observations made over the last decade in the same region as the Fall 2018 EXPORTS field campaign. Our unique method of combining chemical and bio-optical (particle backscatter) sensor data that reflect carbon export over different timescales leverages the information gained from BGC floats, which may help to validate future satellite-based export estimates with in situ data. For example, although biweekly budget-based NCP estimates are useful for investigating seasonal variability in carbon export, when integrated over the entire annual cycle, they provide perspective on regional carbon sequestration (Figure 1). Herein, we discuss the potential application of our approach to other ocean regions via use of new, "fully loaded" BGC Argo floats that carry NO_3^-, O_2, pH, and bio-optical (chlorophyll and backscatter) sensors (Johnson et al., 2017) and consider the opportunity to combine sustained, in situ export estimates with satellite-retrievable parameters in order to monitor

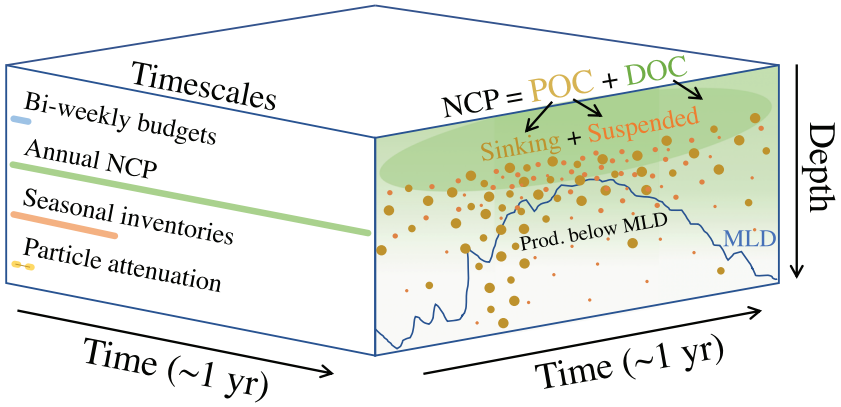

Figure 1. Schematic diagram illustrating the various timescales over which the approaches presented in this paper estimate NCP and POC export rates. The left-hand side shows colored bars with lengths that correspond to the length of time over which each corresponding approach integrates. Our geochemical budgets (blue bar) estimate NCP over approximately 2-week timescales, but by integrating these estimates over the course of a year, we calculate annual NCP (green bar). We also calculate seasonal NCP through time-dependent changes in in situ inventories of chemical tracers (orange bar), as well as particle export across deeper horizons by combining budget-based NCP and estimates of particle depth attenuation using backscatter measurements (yellow bars; two measurements through time are required for each estimate). The right-hand side shows an example annual cycle of relative POC (brown) and DOC (green) concentration with depth produced through NCP at Station Papa (based on actual data shown in Figure 8). The blue line represents the mixed layer depth. Highest particle export typically occurs in the spring as the mixed layer depth shoals, and highest mixed layer particle concentration typically occurs throughout the summer months as the mixed layer is shallowest. We estimate particle attenuation as the difference between depth-integrated particle concentration in the upper water column and specified regions below after a lag time to account for sinking.

future changes in the ocean carbon cycle. Section 2 describes the platforms, sensors, and calibrations used, while section 3 describes the mathematical approaches used to budget each chemical tracer. Section 4 presents the data collected, results of the budget calculations, and a discussion of the limitations of each approach used. Finally, section 5 summarizes the findings and presents concluding remarks.

2. Data

2.1. BGC Argo Floats

Observations presented in this study were measured by six Teledyne/Webb Research APEX BGC profiling floats (ID: 5143, 6400, 6972, 7601, 6881, 7641; WMO #: 5902128, 5903274, 5903405, 5903714, 5903891, 5904125) that were built at the University of Washington and MBARI (Johnson et al., 2010; Riser & Johnson, 2008). The floats were typically programmed to profile from 1,000 m to the surface at ~5-day intervals, giving them a ~4-yr lifetime. They sample at 60 depths between 7 and 1,000 m with 50-m resolution below 400 m, 5-m resolution above 100 m, and 10-m resolution in between. Data analysis was restricted to profiles made within a box bounded by 48.5°N to 53.3°N and 151.5°W to 139°W surrounding the Station Papa mooring (Figure 2). The six float deployments covered approximately nine years (2009–2017), resulting in 18 total years of float data within the box. Nitrate and oxygen data were quality controlled following standard procedures set forth by the international Biogeochemical Argo program (www.biogeochemical-argo.org) and the Southern Ocean Carbon and Climate Observations and Modeling (SOCCOM) project (https://soccom.princeton.edu). All data used can be accessed via the internet (at https://www.mbari.org/science/upper-ocean-systems/chemical-sensor-group/floatviz/).

In addition to a standard Seabird conductivity, temperature, depth (pressure; CTD) sensor package, the floats were equipped with a suite of biogeochemical sensors, including an In Situ Ultraviolet Spectrophotometer (ISUS) optical nitrate sensor (Johnson et al., 2013) produced at MBARI, and an Aanderaa 3830 or 4330 optical O_2 sensor (Tengberg et al., 2006). Two floats also carried WETLabs FLBB optical sensors that measured chlorophyll-a fluorescence (700 nm) and particulate backscatter (700 nm) for 5.5 yr of the study period. Nitrate concentrations were computed from the UV spectra measured by the ISUS sensor with the TCSS algorithm (Sakamoto et al., 2009), and any drift or offset was corrected by comparison to 1,000-m climatological values (Garcia et al., 2010). Oxygen concentrations were computed using

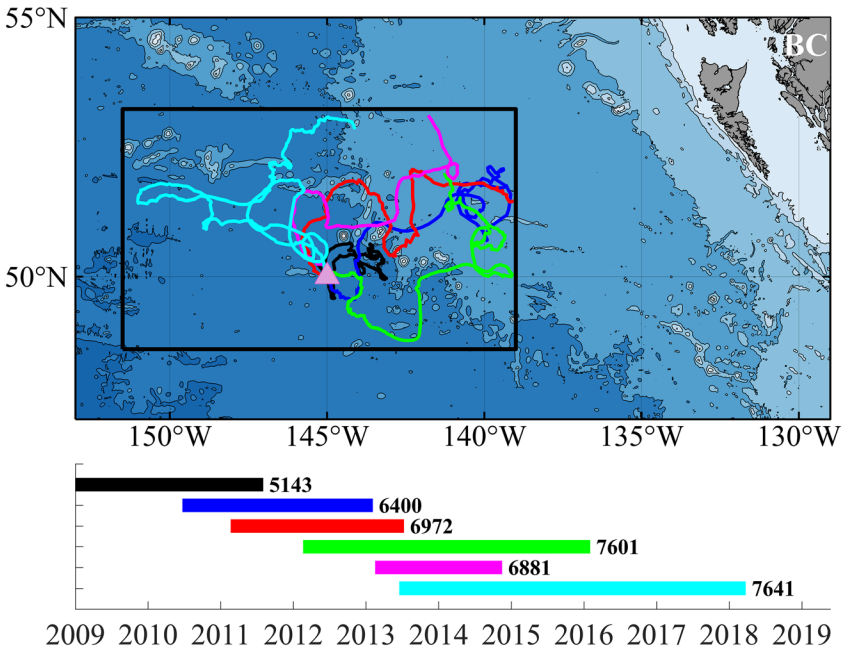

Figure 2. Map of the study region and timeline of float data collection. Colors indicate individual floats, and their identification numbers are listed in bold. The black box in the upper panel indicates the region of float data used. Many of the floats continued to operate outside of this region, but these data were not included in our analysis. Station Papa is shown with a pink triangle. The land mass shown is British Columbia, Canada.

manufacture supplied calibration coefficients, and all floats were corrected for pre-deployment drift. All floats, except for Float 7601, were corrected for in situ drift during deployment using the method of Takeshita et al. (2013), using World Ocean Atlas % O_2 saturation at the surface. Float 7601 was capable of making measurements in air, and thus, in situ drift for this float was corrected using air calibration (Bittig & Körtzinger, 2015; Johnson et al., 2015) using National Centers for Environmental Prediction (NCEP) reanalysis pO_2 at the surface (NCEP reanalysis 1; Kalnay et al., 1996). A comparison of mixed layer properties measured by the floats and bottle samples collected by the Line P program (http://www.waterproperties.ca/linep) in the region is presented by Plant et al. (2016).

2.2. Station Papa Mooring

We leveraged mixed layer measurements of pCO_2 made at the Station Papa mooring (Sutton et al., 2012), as well as measurements of wind speed and pCO_2 made above the sea surface, to close the mixed layer DIC budget. Mixed layer pCO_2 observations and TA values that were calculated using global algorithms based on hydrographic data (discussed below) were used to calculate DIC concentration using CO2SYS (van Heuven et al., 2011) with the constants from Lueker et al. (2000) and Dickson (1990) and the boron-chlorinity ratio of Uppström (1974). The calculation of DIC from pCO_2 and TA has an estimated error of $\pm$3.2 μmol kg^{-1} (Millero, 2007). For consistency, we took daily mean values of all parameters sampled by the mooring and then subsampled this data set to the dates closest to each float profile before making any calculations. At the time of analysis, NOAA Station Papa pCO_2 measurements were available through 2015, so we used the CANYON-B algorithm to calculate mixed layer DIC concentration for the remainder of the data set (through the end of 2017), since the algorithm performed well at this location ($\pm$1 standard deviation of variance from observed values was 13 μmol kg^{-1}; Supporting Information Figure S7).

While the mooring also provides measurements of temperature and salinity at set depth intervals on the mooring line, we found that after careful comparison, the coarse vertical resolution measured on the mooring line caused significant anomalies in vertical gradients compared to those calculated from float measurements, which are integral to NCP calculations (see section 3.3). Instead of attempting to interpolate between mooring sampling depths, we decided to use depth profiles of these variables measured from the floats instead.

2.3. Carbonate System Algorithms

In order to calculate the vertical gradients in TA and DIC below the mixed layer, we tested the accuracy of two recently developed global algorithms for estimating carbonate parameters that apply linear regressions (Carter et al., 2017) and Bayesian neural networks (Bittig et al., 2018). We performed this analysis using GLODAPv2 hydrographic data collected near Station Papa, which was included in the training data set for each algorithm (Figures S1 and S2). Although both algorithms performed nearly identically in this region (each predicted TA to a standard deviation within ± 13 μmol kg^{-1} of concurrent GLODAPv2 measurements, <1% of the magnitude, and 3–6% of the range of values in the upper 1,000 m), CANYON-B was used to calculate TA and DIC gradients for the budget because both DIC and TA can be calculated directly from this algorithm. We use location, pressure, temperature, salinity, and oxygen from float measurements as CANYON-B input variables.

2.4. Satellite-Based NPP and Export

In our analysis, we compare our results to satellite-based estimates of net primary production (NPP) and carbon export. Eight-day NPP estimates from the Vertically Generalized Productivity Model (VGPM) (Behrenfeld & Falkowski, 1997) and the updated Carbon-based Productivity Model (CbPM) (Westberry et al., 2008), as well as ancillary measurements of sea-surface temperature, near-surface chlorophyll-a concentration, and euphotic depth, at 1/6° resolution were downloaded from the Oregon State University's Ocean Productivity website (OSU, 2018). We used the algorithms presented by Laws et al. (2011) and Henson et al. (2011) to calculate POC export ratios (e-ratios; export divided by NPP) from these satellite-derived variables. The Laws et al. (2011) formulation (Equation 3 in that work) relies on euphotic zone nitrate uptake rates (which would include both POC and DOC export), as well as POC export estimates from sediment traps and ^{234}Th budgets for validation (originally presented by Dunne et al., 2005); therefore, this algorithm likely gives an estimate of carbon export that is between total export (POC + DOC) across the euphotic depth and POC export deeper than the euphotic depth. The Henson et al. (2011) algorithm uses data from ^{234}Th budgets in the upper 100 m for validation and therefore gives an estimate of POC export alone across this horizon. POC export was then calculated by mixing and matching the NPP and e-ratio estimates.

2.5. NCEP Reanalysis Winds and Sea Level Pressure Fields

In order to calculate piston velocity at the location of each float, we used a wind speed product from the NCEP (NCEP reanalysis 1; http://www.esrl.noaa.gov/psd/data/gridded/data.ncep.reanalysis.surfaceflux.html; Kalnay et al., 1996) extracted at the position of each float profile. Wind stress curl-driven upwelling velocity was obtained from the Environmental Research Division (ERD) of NOAA (http://las.pfeg.noaa.gov/thredds/dodsC/Model/FNMOC/) and calculated from fields of sea level pressure from the Fleet Numerical Meteorology and Oceanography Center (http://www.usno.navy.mil/FNMOC). Ekman depth and vertical velocity attenuation were calculated following Signorini et al. (2001).

3. Materials and Methods

3.1. Piston Velocity

For estimates of the air-sea flux of CO_2, we first converted 4-m wind speeds measured daily on the Station Papa mooring to 10-m wind speeds using the formulation of Hsu et al. (1994) found in the MATLAB toolbox, gas_toolbox (version 1.0.4), written by C. Manning and D. Nicholson and made publicly available at https://github.com/dnicholson/gas_toolbox (Manning & Nicholson, 2018; Manning et al., 2016). All calculations of gas exchange rate were made using this toolbox. Then piston velocity was calculated using the wind speed-based gas transfer parameterization of Wanninkhof (2014), applying the Schmidt number relationship of Wanninkhof (1992).

3.2. Vertical Turbulent Mixing and Advection

To constrain vertical turbulent mixing rates (K_z) at OSP, we balance chemical budgets over a seasonal timeframe to calculate the mean vertical transport rate using mean rates of seasonal net biological productivity. To do this, we set the mean spring/summer DIC and nitrate budgets for each year (presented below) equal to one another by relating the biological terms through a mean C:N ratio found during spring/summer nutrient consumption (8.2 ± 1.4; Figure 6) while applying the average vertical gradients from the same time period.

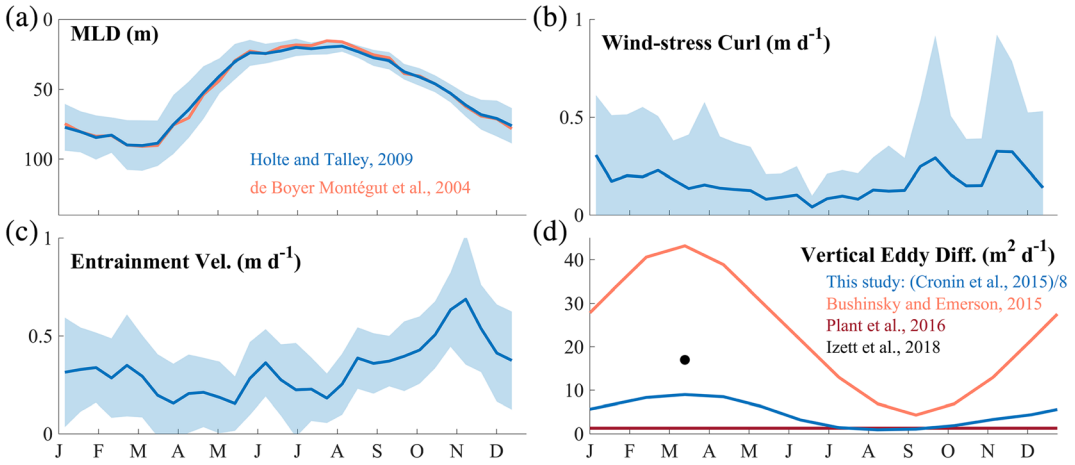

Figure 3. Climatological plots from float data of (a) mixed layer depth using the algorithm of Holte and Talley (2009) and a density threshold of 0.03 kg m^{-3} from the upper 10-m density (de Boyer Montégut et al., 2004), (b) wind stress curl-driven vertical advection, (c) entrainment velocity, and (d) vertical eddy diffusivity at the base of the mixed layer. The dark blue line in (a)–(c) is the mean value in 2-week intervals over an annual cycle from 2009 to 2017, and the light blue cloud represents 1 standard deviation of all years. In panel (d), the blue line is the eddy diffusivity used in this study, which is equivalent to the Cronin et al. (2015) heat budget result divided by 8, but following the same seasonal cyclicity. Shown in orange and red are the values used in similar float studies near Station Papa, Bushinsky and Emerson (2015) and Plant et al. (2016), respectively. Shown with a black dot is an upper limit for spring eddy diffusivity estimated at the base of the mixed layer by Izett et al. (2018) at OSP.

This gives a constraint on the total vertical physical transport term, which we then partition into turbulent diffusive mixing, wind stress curl-driven advection, and entrainment and solve for a mean K_z rate. Although there is considerable uncertainty in the C:N ratio (~20%), it is most likely due to interannual variability, and this approach provides a direct estimate on turbulent mixing rates, which routinely span orders of magnitude. Our estimates were compared to those of Cronin et al. (2015) who balanced a mixed layer heat budget using data from the OSP mooring. Our budget method suggests a mean spring/summer value that is approximately eight times lower than Cronin et al. (2015) (Figure 3d). One reason for this disagreement may stem from the spacing of the sensors on the mooring array, as we found that, especially during periods of the year when the mixed layer was deep, budgets using the mooring sensors often disagreed with those made from the higher-resolution float-based measurements. Because our approach only gives a single seasonal value, we apply the seasonality found by Cronin et al. (2015) to our resulting K_z value, similar to the approach of Bushinsky and Emerson (2015) who used K_z values of approximately four times less than Cronin et al. (2015). Izett et al. (2018) estimated an upper limit on K_z at OSP (total vertical transport due to mixing, advection, and entrainment) in spring of approximately 17 m^2 day^{-1} by budgeting the mixed layer inventory of N_2O with losses due to air-sea gas exchange and supply from below. This estimate is approximately 50% greater than our estimate of K_z in spring (~10 m^2 day^{-1}) but is still less than that of Bushinsky and Emerson (2015).

Entrainment velocity was calculated as the change in mixed layer depth (MLD) through time, defined using the algorithm of Holte and Talley (2009). Typically, MLD is calculated at Station Papa using a density threshold of 0.03 kg m^{-3} from a mean of the upper 10 m (de Boyer Montégut et al., 2004), which is in close agreement with the Holt and Talley algorithm in this region (Figure 3a). Entrainment velocity at our study location ranged from ~0.25 to 0.75 m day^{-1} on average when presented as a climatology over the entire study (Figure 3c) but is negative during times of mixed layer shoaling. The presentation in Figure 3c neglects any negative values, causing our entrainment velocity climatology to be skewed positive. This is due to our model formulation where we set negative entrainment velocities to zero during mixed layer shoaling to avoid biasing the flux calculations in our budgets, as the change in tracer inventory during mixed layer shoaling is accounted for by the change in MLD. Wind stress curl is another possible source of vertical advection, and estimates were accessed through NOAA ERD, as described above (Figure 3b).

3.3. NCP From Budgets of DIC, TA, and NO_3^-

The following chemical budgets are one-dimensional and assume that vertical fluxes are dominant while horizontal gradients throughout our study region are negligible, which has been shown previously (Fassbender et al., 2016; Plant et al., 2016). The following budgets of three biogeochemical tracers (DIC, TA, and NO_3^-) are evaluated in a one-box model with different heights, initially in the surface mixed layer (variable through time), but we also apply the same calculations in three other depth zones, the euphotic zone (using monthly climatological mean depths estimated from float observations; ~54–60 m; Figure S3), the 100-m horizon (constant), and the maximum MLD (calculated for each year individually, but variable from year to year). The only difference between these budgets is in regard to the transport terms. For all budgets other than the mixed layer, entrainment velocity becomes zero, negating this term in the budget. For the euphotic zone budget, eddy diffusivity is set to the annual mean used for the mixed layer budget (4.6 m^2 day^{-1}), since the euphotic depth is approximately the mean MLD at this location. Also, for the 100-m and maximum MLD budgets, we assume that the influence of wind stress curl-driven advection is negligible and eddy diffusivity is set to 1.3 m^2 day^{-1}, the same as Plant et al. (2016) and approximately the minimum value used for the mixed layer budget.

In order to evaluate the equations presented below numerically, we are required to take derivatives of observational sensor-based data, which is inherently noisy in nature. In addition, profiling floats are particularly susceptible to biases associated with vertical tidal motions that are difficult to remove because of their low profiling frequency (~weekly). This necessitates a filtering and smoothing protocol to dampen noise that is not representative of the mean environmental signal. We chose to smooth the mixed layer concentration of each tracer and the change in concentrations through time by using a running three-point mean to remove some of the higher-frequency variability in the signal when evaluating the following equations. Furthermore, we present the budget results as a climatology throughout the manuscript in order to leverage the large amount of available data at this location and reduce the overall uncertainty in our analysis of the annual cycle of NCP. Because we are interested in the mean state of the regional ecosystem throughout this decade, we use a time-dependent average of all float years (e.g., if three floats collected data in 2014, each float year contributes independently to the climatology) at ~2-week intervals throughout each annual cycle. We also tested whether interannual variability in NCP biased our climatological results by first averaging all data from each calendar year but found the ANCP to be within our reported uncertainty using either method (Figure S4). The only time that annual composites of float observations from the same year are used is in section 4.3 to determine profiles of remineralization rate estimates.

3.3.1. Dissolved Inorganic Carbon

We used a DIC budget (calculated from pCO_2 and TA) to calculate the biological component contributing to the change in DIC over time (t), following the formulation of Fassbender et al. (2016):

$$\frac{\partial DIC}{\partial t} = \left.\frac{\partial DIC}{\partial t}\right|_{Gas} + \left.\frac{\partial DIC}{\partial t}\right|_{Phys} + \left.\frac{\partial DIC}{\partial t}\right|_{EP} + \left.\frac{\partial DIC}{\partial t}\right|_{Bio} \quad (1)$$

where the subscripts *Gas*, *Phys*, *EP*, and *Bio* refer to the gas exchange, physical variability, evaporation/precipitation, and biological components contributing to the DIC budget, respectively. The following sections address our approach to constraining each of these terms to solve for the biological contribution.

The gas exchange term (first term on the right-hand side of the equation) is defined as

$$\left.\frac{\partial DIC}{\partial t}\right|_{Gas} = k * K_H * \Delta pCO_2 \quad (2)$$

where k is the piston velocity, K_H is the solubility constant of CO_2, Weiss (1974), and $\Delta pCO_2 = pCO_{2\ sea} - pCO_{2\ atm}$. The second term on the right-hand side of Equation 1 represents the change in DIC through time due to physical variability in the surface ocean:

$$\left.\frac{\partial DIC}{\partial t}\right|_{Phys} = -\left(w + \frac{\partial h}{\partial t}\right)\left(\frac{DIC_{ML} - DIC_h}{h}\right) - \frac{K_z}{h}\left(\frac{\partial DIC}{\partial z}\right) \quad (3)$$

where DIC_{ML} is DIC concentration in a mixed layer of depth h, and w, DIC_h, K_z, and $\delta DIC/\delta z$ are the

vertical velocity, DIC concentration, eddy diffusivity, and vertical concentration gradient evaluated at the depth of the mixed layer.

The effects of evaporation and precipitation on the surface ocean DIC budget are calculated using the following:

$$\left.\frac{\partial DIC}{\partial t}\right|_{EP} = \left(\frac{\partial Sal}{\partial t} - \left.\frac{\partial Sal}{\partial t}\right|_{Phys}\right) * \left.\frac{DIC}{Sal}\right|_{t=1} \tag{4}$$

By rearranging Equation 1, we then solve for the biological component to the change in DIC through time, which is equivalent to the sum of the contributions from NCP and the formation of $CaCO_3$:

$$\left.\frac{\partial DIC}{\partial t}\right|_{Bio} = \left.\frac{\partial DIC}{\partial t}\right|_{NCP} + \left.\frac{\partial DIC}{\partial t}\right|_{CaCO_3} \tag{5}$$

3.3.2. Total Alkalinity

Because TA is influenced by all the same processes as DIC, except gas exchange, we can use the previous equations to budget TA, as well (Wolf-Gladrow et al., 2007):

$$\frac{\partial TA}{\partial t} = \left.\frac{\partial TA}{\partial t}\right|_{Phys} + \left.\frac{\partial TA}{\partial t}\right|_{EP} + \left.\frac{\partial TA}{\partial t}\right|_{NCP} + \left.\frac{\partial TA}{\partial t}\right|_{CaCO_3} \tag{6}$$

which, after calculating the physical and evaporation/precipitation terms identically to the DIC budget, also simplifies to

$$\left.\frac{\partial TA}{\partial t}\right|_{Bio} = \left.\frac{\partial TA}{\partial t}\right|_{NCP} + \left.\frac{\partial TA}{\partial t}\right|_{CaCO_3} \tag{7}$$

Biological processes influence DIC and TA at known stoichiometric ratios. For instance, for every mole of $CaCO_3$ produced, a reduction of 1 mole of DIC and 2 moles of TA occurs. Organic matter production consumes 1 mole of phosphate, 18 moles of H^+, and 117 moles of CO_2, causing a 17-mole increase in TA (Anderson & Sarmiento, 1994). Therefore, we are able to rearrange Equations 5 and 7 to close the budget:

$$\left.\frac{\partial DIC}{\partial t}\right|_{NCP} = \frac{\left(\left.\frac{\partial TA}{\partial t}\right|_{Bio} - 2 * \left.\frac{\partial DIC}{\partial t}\right|_{Bio}\right)}{\left(-2 + \frac{-17}{117}\right)} \tag{8}$$

$$\left.\frac{\partial DIC}{\partial t}\right|_{CaCO_3} = \left.\frac{\partial DIC}{\partial t}\right|_{Bio} - \left.\frac{\partial DIC}{\partial t}\right|_{NCP} \tag{9}$$

The last equation represents the production of $CaCO_3$, or PIC, by calcifying organisms in the surface ocean.

3.3.3. Nitrate

Nitrate can also be budgeted in the surface ocean, similar to the approach of Plant et al. (2016):

$$\frac{\partial NO_3}{\partial t} = \left.\frac{\partial NO_3}{\partial t}\right|_{Phys} + \left.\frac{\partial NO_3}{\partial t}\right|_{EP} + \left.\frac{\partial NO_3}{\partial t}\right|_{NCP} \tag{10}$$

where each term is formulated as in the DIC budget. Of the six floats used in this study, one has anomalously high standard deviation in the nitrate data due to low light throughput in the nitrate sensor, perhaps due to damage incurred during transit or deployment (ID: 6400; Plant et al., 2016). The effect was most apparent during 2012 and can been seen in Figure 4 (dark blue points). As a result, data from this float were neglected in all calculations using nitrate data. This did not affect our temporal coverage, as two other floats overlapped during the entire lifetime of Float 6400 (Figure 2).

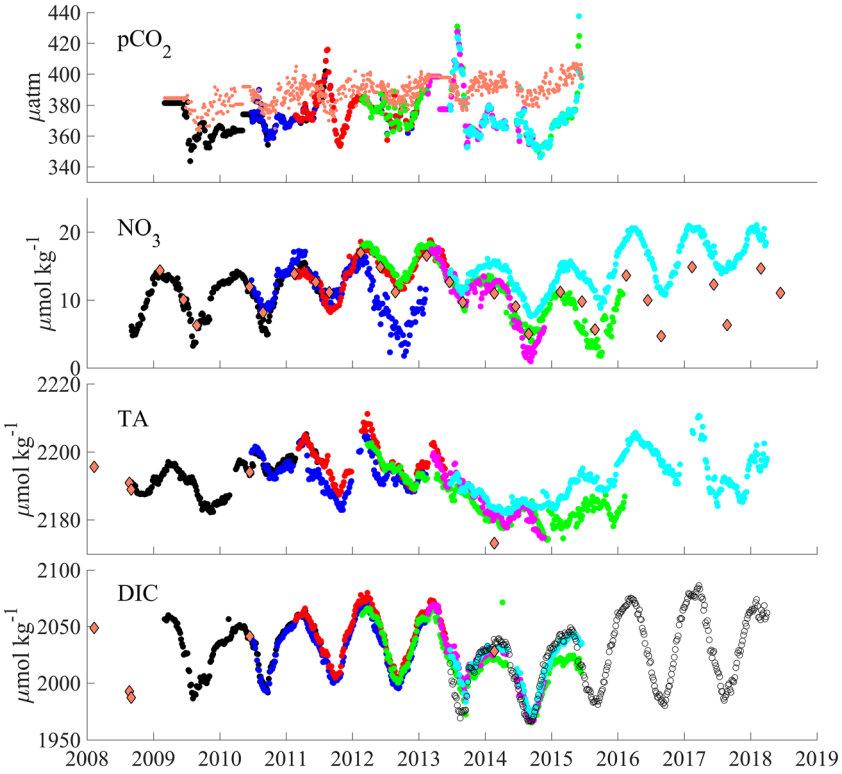

Figure 4. The data sets used to calculate mixed layer NCP in this study. Mixed layer (colors) and air (salmon dots) pCO_2 measured on the NOAA Station Papa mooring (accessed via www.noaa.gov) subsampled to the float sampling frequency, nitrate measured by floats, TA calculated from float-measured pressure, temperature, salinity, and oxygen using the CANYON-B algorithm (Bittig et al., 2018), and DIC calculated from TA and pCO_2 using CO2SYS. Colors indicate floats and correspond to the colors in Figure 2. The open symbols in the bottom panel indicate DIC calculated using CANYON-B for Float 7641, which we used during the time period when mooring pCO_2 data were unavailable. Solid diamonds are discrete measurements made in our sampling region by the Line P program (accessed via www.dfo-mpo.gc.ca).

3.4. POC and DOC Decomposition

In order to partition the NCP term, we assume that NCP is the sum of two quantities: the production rate of the POC portion and of the DOC portion.

$$\left.\frac{\partial NO_3}{\partial t}\right|_{NCP} = \left.\frac{\partial NO_3}{\partial t}\right|_{POC} + \left.\frac{\partial NO_3}{\partial t}\right|_{DOC} \tag{11}$$

Once the nitrate and DIC budgets are solved for NCP, they can be related via a unique C:N ratio in each organic matter pool. We can then substitute DIC terms into the nitrate equation and expand, as follows:

$$\left.\frac{\partial NO_3}{\partial t}\right|_{NCP} = \frac{1}{C{:}N_{POC}} * \left.\frac{\partial DIC}{\partial t}\right|_{POC} + \frac{1}{C{:}N_{DOC}} * \left.\frac{\partial DIC}{\partial t}\right|_{DOC} \tag{12}$$

$$\left.\frac{\partial NO_3}{\partial t}\right|_{NCP} = \frac{1}{C{:}N_{POC}}\left(\left.\frac{\partial DIC}{\partial t}\right|_{NCP} - \left.\frac{\partial DIC}{\partial t}\right|_{DOC}\right) + \frac{1}{C{:}N_{DOC}} * \left.\frac{\partial DIC}{\partial t}\right|_{DOC} \tag{13}$$

$$\left.\frac{\partial NO_3}{\partial t}\right|_{NCP} = \frac{1}{C{:}N_{POC}} * \left.\frac{\partial DIC}{\partial t}\right|_{NCP} - \frac{1}{C{:}N_{POC}} * \left.\frac{\partial DIC}{\partial t}\right|_{DOC} + \frac{1}{C{:}N_{DOC}} * \left.\frac{\partial DIC}{\partial t}\right|_{DOC} \tag{14}$$

$$\left.\frac{\partial NO_3}{\partial t}\right|_{NCP} = \frac{1}{C{:}N_{POC}} * \left.\frac{\partial DIC}{\partial t}\right|_{NCP} + \left(\frac{1}{C{:}N_{DOC}} - \frac{1}{C{:}N_{POC}}\right) * \left.\frac{\partial DIC}{\partial t}\right|_{DOC} \tag{15}$$

We can then solve for the DOC portion in terms of NCP and the two prescribed nutrient ratios:

Table 1
Total ANCP Estimates and Nutrient Ratios From Budgets and Seasonal Production/Remineralization Rates

	Tracer budgets (all in mol m^{-2} yr^{-1})			Nutrient ratios	
Depth zone	O_2	DIC	NO_3	O:C	C:N
Mixed layer (ANCP; Figures 5a and 5b)	-	2.1 ± 1.0	0.27 ± 0.13	-	7.8 ± 3.0
Euphotic zone (ANCP; Figures 5c and 5d)	-	2.0 ± 0.6	0.22 ± 0.07	-	8.8 ± 3.5
Euphotic zone (spring; Figure 6)[a]	-	2.0 ± 0.2	0.24 ± 0.04	-	8.2 ± 1.4
Z_{eu} to 100 m (fall; Figure S10)[a]	−3.9 ± 1.2	2.3 ± 0.7	0.34 ± 0.24	1.76 ± 0.25	7.4 ± 3.7
Z_{eu} to 200 m (fall; Figure S10)[a]	−6.2 ± 2.3	4.0 ± 1.7	0.76 ± 0.66	1.46 ± 0.26	6.2 ± 3.4

Note. Uncertainties reported for ANCP values were determined using the Monte Carlo approach, whereas the uncertainties reported for spring and fall production/remineralization and nutrient ratios were determined as the standard deviation of the values for individual years.
[a]Estimated as the change in in situ inventories in O_2, DIC, and NO_3^- (shown in Figure 6) during the spring or fall season (~1/3 of the year) divided by 3 to estimate an annual mean rate of net production, assuming that there is no other net production throughout the year.

$$\left.\frac{\partial DIC}{\partial t}\right|_{DOC} = \frac{\left.\frac{\partial NO_3}{\partial t}\right|_{NCP} - \frac{1}{C{:}N_{POC}} * \left.\frac{\partial DIC}{\partial t}\right|_{NCP}}{\frac{1}{C{:}N_{DOC}} - \frac{1}{C{:}N_{POC}}} \tag{16}$$

We then calculate the POC fraction by difference:

$$\left.\frac{\partial DIC}{\partial t}\right|_{POC} = \left.\frac{\partial DIC}{\partial t}\right|_{NCP} - \left.\frac{\partial DIC}{\partial t}\right|_{DOC} \tag{17}$$

Using this formulation, we isolate the POC and DOC portions of NCP. As a result of this approach being unable to distinguish between sinking and suspended particles, all particle production through NCP is included in the POC term. Because the portion that is suspended has not been exported through sinking, this makes our POC NCP and total NCP estimates upper limits, but likely within our reported uncertainty. Of course, this approach is dependent on determining the ratio of carbon to nitrogen in each of the organic carbon pools. Therefore, we rely on two approaches to constrain the C:N ratios: (1) measurements made on filtered particles (2018/2019), DOC and dissolved organic nitrogen (DON) (2017) collected during 3 Line P program cruises to the study region at different times of the year (Bif & Hansell, 2019), and (2) in situ changes through time in the euphotic zone inventories of DIC and nitrate during spring production and beneath the euphotic zone during fall remineralization of organic matter (bottom half of Table 1). We also cite literature values in support of our results.

Sinking particles caught in sediment traps at OSP typically have a higher C:N ratio than we chose to represent particulate organic matter (POM) produced during net production in the surface ocean (~8 at 50–100 m and increasing with depth, Timothy et al., 2013; Wong et al., 1999). This is because nitrogen is preferably scavenged by heterotrophic organisms as particles sink, and suspended particles in the surface ocean have a much lower C:N ratio (~5.5 ± 0.2; mean from 3 cruises between September 2018 and August 2019 during this study). Therefore, the C:N in total POM being produced in the surface ocean is likely near Redfield stoichiometry (6.6), assuming that suspended and sinking particles are produced at approximately equal proportions. Thus, we use 6.6 ± 1 in our budgets as the C:N in POM produced during this study (±1 represents the middle 80% of the total range of 2.5).

Dissolved organic matter (DOM) concentrations have been measured at OSP (Bif & Hansell, 2019), and through discussions with these authors, as well as with C. Carlson and B. Stephens (UCSB), we use a value of 14 ± 1 for the C:N of DOM production in our budgets (midpoint of 12.5 and 15; ±1 includes 80% of this range). Although there is likely seasonality in the DOM pool, we have not imposed any variability in the C:N ratio for two reasons: (1) Its magnitude has not been quantified nor the role of entrainment of deep waters high in DOC and low in DON into the surface ocean during winter mixing (Bif & Hansell, personal communication), and (2) the C:N ratio in DOM during its production is likely unique from the C:N in ambient DOM given the differences in lifetimes in the water column of DOC and DON (Carlson & Stephens, personal communication). Because nutrient ratios were not measured throughout the entirety of float deployments, the DIC- and nitrate-based NCP rates may lag each other in time, and some outliers do

exist. We filtered our results by neglecting any values with total C:N (calculated by taking the DIC-derived NCP divided by the nitrate-derived NCP) less than 0 or greater than 15 (found to be the case for 2 out of 32 points in the mixed layer budget climatology) or any values where the POC portion of NCP was larger than total NCP (found for 7 points). The former were considered outliers and ignored, while the latter were set equal to total NCP.

3.5. Uncertainty Analysis

Uncertainty in our budget results was determined using a Monte Carlo approach, which calculates NCP for each float year with 10,000 simulations of randomly selected values within ±1 standard deviation for each of the most important flux contributors in the chemical mass balance. The important flux contributors and their uncertainties are vertical advection (±35% determined through balance of physical fluxes, described above), vertical diapycnal eddy diffusivity (±35% for the mixed layer budget and ±70% for the euphotic zone budget, as this is not consistent with other physical boundaries), the C:N ratios used for POM and DOM (±1; the approximate standard deviation of estimates), concentrations and gradients of DIC, TA (±13 μmol kg^{-1}; ±2 nmol kg^{-1} m^{-1}), and NO_3^- (±0.5 μmol kg^{-1}; ±0.1 nmol kg^{-1} m^{-1}), determined as the uncertainty of the carbonate system parameter algorithm in the region and measurement uncertainty of the ISUS (Figures S1, S2, and S6), and the euphotic zone depth (±6 m; Figure S3). The upper and lower bounds for NCP were then calculated as 1 standard deviation from the best estimate of all simulations, determined as the percentile between which 16% and 84% of the simulated production rates were distributed. A sensitivity analysis of each of the contributions to the overall uncertainty in ANCP was performed by running the Monte Carlo simulation with each of the contributors to overall uncertainty individually. The results of this analysis are presented in the supporting information (Table S1) and discussed in section 4.2.

4. Results

4.1. Float NO_3, Mooring pCO_2, TA, and DIC Records

Figure 4 presents the data sets used in the NCP budgets in this study. Plant et al. (2016) and Fassbender et al. (2016) have previously presented mixed layer values of nitrate, oxygen, DIC, and TA in this region through 2015. This data set extends those previous observations by about 2 yr. Additionally, the TA values presented here are calculated by the CANYON-B algorithm, whereas the TA values presented by Fassbender et al. (2016) were calculated by the authors using a salinity relationship, though the results are similar (Figure S2). DIC presented here is calculated from pCO_2 measurements and TA values from CANYON-B. Since mooring pCO_2 data were unavailable after 2015, we used DIC calculated from CANYON-B in the budget from 2015 to 2018 (open symbols; Figure 4) and present these values from 2013 to 2018 to emphasize the agreement with values calculated from pCO_2 and TA.

During 2014 and 2015, the Northeast Pacific experienced anomalously high temperature and low salinity (Di Lorenzo & Mantua, 2016), as well as low nitrate, TA, and DIC concentrations, which is apparent in our data set (Figure 4). Yang et al. (2018) investigated interannual ANCP variability during these years using O_2 and DIC budgets in this region and found that NCP initially decreased in 2014, then returned to pre-anomaly values in 2015, and that the oxygen budget was much more sensitive to this interannual variability than DIC. Another striking feature of the data is the apparent positive trend in nitrate, TA, and DIC that deviates from the discrete samples measured at Station Papa after 2015 when only Float 7641 was sampling (cyan colored points in Figure 4). This deviation from the decadal mean was also observed in temperature and salinity (not shown here; see Plant et al., 2016) and was concurrent with this float moving north within the study area, which is toward a known high-nutrient, low-chlorophyll (HNLC) region in the Gulf of Alaska where nitrate can accumulate in the surface waters (Martin & Fitzwater, 1988). Due to this, we believe this signal is not a result of sensor drift, but spatial variability in the water mass properties sampled; thus, a horizontal gradient must exist within the northern part of our study region. Because there was no discernable variability in production rates during this portion of the study period (Figure S5), we chose to include these years in the analysis presented.

4.2. NCP Across Various Depth Horizons

The climatology of NCP estimated from all float years using the mixed layer budgets of DIC (Figure 5a) and nitrate (Figure 5b) shows that the two tracer budgets have a similar seasonality, peaking in the spring

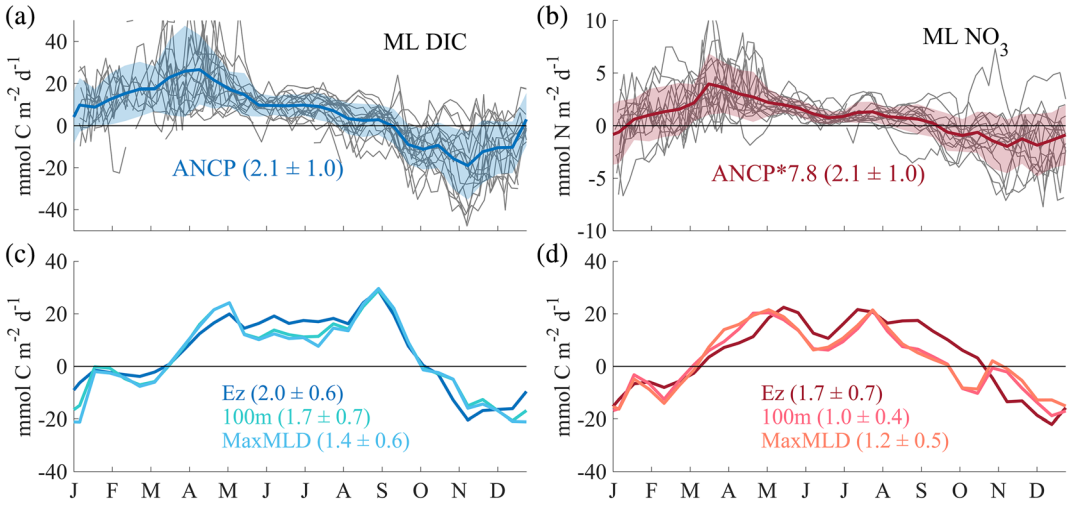

Figure 5. Mixed layer climatological mean (dark lines) and 1 standard deviation (cloud) of net community production (NCP; in mmol C m^{-2} day^{-1}) for all float years (gray lines) from the (a) DIC budgets (blue) and (b) nitrate budgets (red; in mmol N m^{-2} day^{-1}). (c, d) Same as (a, b), but mean results for the budgets evaluated to the following depth horizons: euphotic depth (*Ez*), 100 m, and maximum mixed layer depth for each year (MaxMLD). The values in parentheses are the integrated annual NCP rates for each budget and uncertainty evaluated using the Monte Carlo approach (all in mol C m^{-2} yr^{-1}; nitrate-based values use a C:N of 7.8 to convert into carbon units).

(March–April) before decreasing almost linearly into net heterotrophy in the fall/winter (October–December). Interestingly, once a constant depth horizon was used (approximately constant for the euphotic zone [54–60 m], 100 m, and annual maximum MLD), the seasonality shifted, with NCP occurring later in spring and slightly later net heterotrophy in fall. Additionally, the budgets display two evenly distributed peaks in the spring and summer for nitrate, and slightly earlier and later peaks for the DIC budgets (Figures 5c and 5d). These characteristics arise from the fixed depth horizons always being deeper than the MLD, except during winter. In other words, the mixed layer is shallower than the fixed depth horizons during more productive periods and deeper during less productive periods.

ANCP, presented in parentheses in Figure 5 (all in mol C m^{-2} yr^{-1}) and Table 1, represents the total amount of NCP over the annual cycle and is calculated by integrating under the NCP curves. It is important to note that in Figure 5 we use a constant C:N of 7.8, which we found by balancing the mixed layer ANCP estimates (Figures 5a and 5b), and then apply this to all nitrate-based depth horizon budgets and ANCP estimates presented in Figures 5c and 5d. We recognize that NCP likely occurs with a variable C:N over time and at various depth intervals and this will be discussed in the following sections. We chose to use a constant C:N for this calculation in order to make a direct comparison between the two tracer budgets. The values calculated directly from the nitrate budget are presented in Table 1. As expected, the ANCP estimates decrease with integration depth, as increasingly more dark, net heterotrophic depths beneath the euphotic zone are included in the budgets. The only discrepancy to this pattern is that the max MLD nitrate budget ANCP is slightly larger than the 100-m budget (by 0.2 mol C m^{-2} yr^{-1}), but this is well within the uncertainty of the estimate, and the average max MLD over the decade is ~105 m. The main difference between how the MLD and other budgets are calculated in this study is that the depth of integration is variable when calculating a mixed layer budget.

The clouds presented in Figures 5a and 5b represent 1 standard deviation from the mean of NCP in each ~2-week interval for all float years presented. This presentation is useful in illustrating the variance between all of the annual cycles used to calculate the decadal mean NCP climatology. Of course, any interannual variability is also included in the spread between float years, and thus, this approach may be insufficient to accurately estimate the uncertainty in the NCP climatology produced from the entire data set. Therefore, we also use a Monte Carlo approach to calculate uncertainty in the mean of each ~2-week interval (Figures S8 and S9) and the ANCP calculated for the climatology (values in parentheses in Figure 5). The resulting overall estimate for uncertainty in mixed layer ANCP over this decade is ±1.0 mol C m^{-2} yr^{-1} and ±0.6 mol

C m^{-2} yr^{-1} in our euphotic zone budget. For comparison, Fassbender et al. (2016) reported an uncertainty of ±1 mol C m^{-2} yr^{-1} and Plant et al. (2016) reported an uncertainty of ±0.6 mol C m^{-2} yr^{-1} using mixed layer DIC/TA and upper 35-m nitrate mass balances to calculate ANCP, respectively. Using oxygen mass balances, Emerson and Stump (2010) reported an uncertainty of ±1 mol C m^{-2} yr^{-1} in the surface mixed layer and Yang et al. (2018) reported an uncertainty of ±0.7 mol C m^{-2} yr^{-1} in the upper ~100 m. Our uncertainty estimate is similar to those previously reported for this region using similar approaches. One reason we are able to successfully apply this method to this region is due to the large amount of data collected via floats over this decade (~18 total years of data), which reduces the overall uncertainty when using a climatology-based approach. We also present the results of the Monte Carlo simulation after varying each of the contributors to uncertainty individually (Table S1). The largest contributors to overall ANCP are the eddy diffusivity rate, advection rate, and DIC gradient, whereas the POC and DOC splits are also sensitive to the choice of C:N ratios, nitrate concentration, and nitrate gradient. It is important to note that as a result of competing and/or interrelated terms in the overall budget, the total uncertainty (determined by varying all contributing terms) is similar to that introduced through the physics terms alone (the largest contributors). This suggests that errors may be correlated such that uncertainty estimated by propagating individual error terms under the assumption that they are uncorrelated may overestimate the true total uncertainty. Furthermore, the euphotic zone budgets, as well as the deeper zone budgets, have smaller uncertainty than the mixed layer because using a constant, or near-constant, depth horizon greatly reduces the magnitude of the physical terms.

Although we could have used an oxygen budget to estimate NCP as well, nitrate, DIC, and TA budgets were chosen for this study due to our interest in euphotic zone NCP and the sensitivity of oxygen budgets on accurate gas exchange rates at the air-sea interface, which has been addressed in a previous manuscript using the same float data set (Plant et al., 2016). Furthermore, oxygen has been used as a tracer of NCP in the Northeast Pacific in many previous studies (Bushinsky & Emerson, 2015; Emerson & Stump, 2010; Emerson et al., 2008, 2019; Nicholson et al., 2008; Pelland et al., 2018; etc.); thus, we believe our oxygen budget analysis provides no further insight to the contributions cited.

4.3. Nutrient Ratios, Biological Production, and Remineralization Rate Estimates From Inventories

To first order, we can estimate seasonal biological production rates in the euphotic zone by plotting DIC and NO_3^- inventories through time, then using a least squares linear regression over each spring/summer season (April through August) to calculate a mean rate of drawdown through net biological consumption during this time of year (Figure 6 and Table 1). In doing so, we must assume that all NCP occurs during this portion of the year because this is the only period of inventory drawdown throughout the year. We neglect oxygen in this analysis due to the large effect of air-sea exchange on the near-surface inventory, and note that we do not make a correction for gas exchange on the DIC inventory because this effect was estimated to be within the uncertainty of this approach and due to the time it takes for CO_2 to exchange with the DIC reservoir to achieve chemical equilibrium with atmospheric CO_2 in the region being on the order of a year (Broecker & Peng, 1974; Yang et al., 2018), this correction would likely introduce unnecessary uncertainty into our calculation. Additionally, we exclude three years of fits (2010, 2011, and 2017) from the averaging in which calculated total C:N fell outside of the range we designate as reasonable (0–15). In each of these three years, the seasonal fit was greater than 15. One caveat to this approach is that the MLD fluctuates between being above and below the euphotic depth throughout the year at this location; thus, its depth has an effect on the concentration and inventory of each of these parameters in the euphotic zone, so some of the variability may be due to this effect, as well as air-sea exchange, which we neglect in assuming that the variability is due to biological production alone. Nevertheless, we use the resulting mean ratio (8.2 ± 1.4) as an indication of likely total C:N ratios during organic material production in the region, and this supports the value used in our budget calculations (7.8; Figure 5).

To estimate remineralization rates and the elemental ratios in organic material as it is remineralized, we plot the change in DIC, NO_3^-, and O_2 along each 0.05 kg m^{-3} of isopycnal beneath the euphotic zone (Figure S10), similar to the approach of Hennon et al. (2016). In making this calculation, we assume that the majority of remineralized material is sourced locally. Thus, the change in concentration over time along water mass isopycnals that are not locally ventilated gives an estimate of the biological consumption or

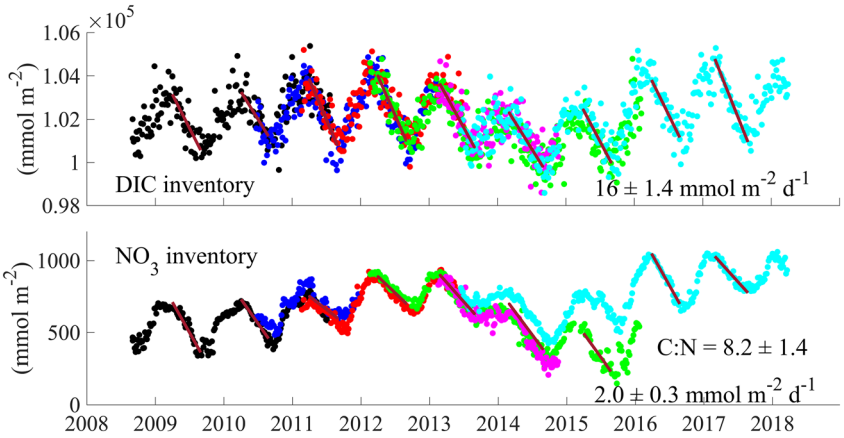

Figure 6. Euphotic zone inventories of DIC and nitrate plotted through time. Least squares linear regressions from April through August are shown in dark red. The mean slope and standard deviation of these regressions are shown on each plot, neglecting three outlier years (2010, 2011, and 2017).

production of the chemical tracer. Integrating the profiles of production/consumption in two depth zones (Z_{eu} to 100 m and Z_{eu} to 200 m) gives us an estimate of the rate and nutrient ratios of remineralization in these depth zones (Table 1). In our integrations, we neglect any values that would indicate production of new organic material (i.e., positive changes in oxygen or negative changes in DIC or nitrate), as this is most likely indicative of lateral transport and not biological in origin. This was only a significant problem throughout the fall of 2015.

The bottom half of Table 1 summarizes the results of in situ production rate estimates and nutrient ratios. The euphotic zone estimates of ANCP agree with those calculated from the DIC and nitrate budget approaches, well within the estimated uncertainties. Remineralization rates beneath the euphotic zone and above 100 m agree within uncertainty with ANCP from the euphotic zone, but remineralization rates calculated from the euphotic depth to 200 m are greater than calculated ANCP above the euphotic depth. If the system is one-dimensional, then these are likely overestimates of total remineralization. However, lateral transport could also bias these estimates by contributing to the change through time of tracer concentrations in the water column, or by introducing a water mass that acquired organic matter produced elsewhere. Regardless of a non-local source of material, we can assess nutrient ratios during remineralization by assuming that organic matter is of similar composition throughout the region. NCP C:N ratios (right side of Table 1) decrease with increasing depth from larger than Redfield in the near-surface to near-Redfield on average between the euphotic depth and 200 m. As discussed in section 3, POM produced during NCP likely has a lower C:N than sinking particles (~8; Wong et al., 1999) due to preferential nitrate remineralization, but the production of DOM likely has a much higher C:N (~12.5–15; Letscher et al., 2015). Therefore, the C:N of total organic matter produced during NCP is likely larger than Redfield (~6.6), but the C:N during remineralization beneath the euphotic zone should decrease with depth as an increasing proportion of organic matter is sourced from particles. This is what we observe and supports of our choice for end-member C:N values for POM (6.6) and DOM (14) during NCP in the tracer budget analysis.

4.4. Particulate and Dissolved Portions of Mixed Layer NCP and PIC Production

The climatological results of our mathematical decomposition of NCP into POC and DOC pools for the mixed layer and euphotic zone budgets, as well as integrated ANCP, are presented in Figures 7a and 7b. Overall, POC was approximately 76% (±38%) and 70% (±25%) in the mixed layer and euphotic zone budgets, respectively. Thus, the DOC portions were about 24% (±28%) and 30% (±10%) of total NCP, similar to previous estimates of net DOC production in the surface ocean (Bif & Hansell, 2019; Carlson et al., 1994; Hansell et al., 2009). Our estimate of net PIC production follows the same general seasonal pattern and the annual net production rate (0.1–0.3 mol C m^{-2} yr^{-1}) is in agreement, within uncertainty, with previously published results at this site (0.3 ± 0.3 mol C m^{-2} yr^{-1}; Fassbender et al., 2016). One noticeable feature is that the relative proportions of POC and DOC in NCP vary significantly throughout the year. DOC appears to be

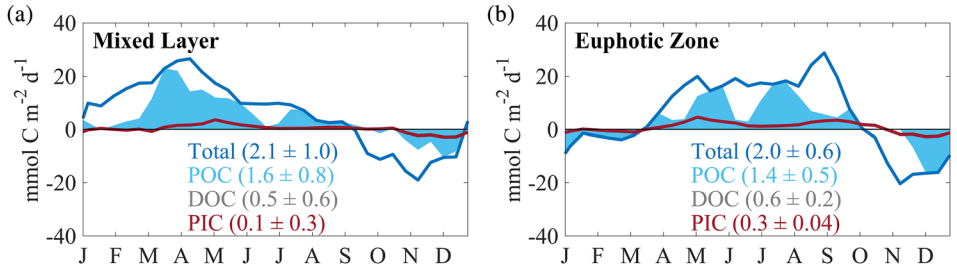

Figure 7. Climatological mean NCP over the entire study period (2009–2017; blueline), the POC portion of NCP (filled blue area), the DOC portion (white space), and PIC production rate (red line), in (a) the mixed layer and (b) the euphotic zone. The numbers in parentheses are the integrated annual NCP rates for each curve, and uncertainty reported was determined using a Monte Carlo approach. The time-varying uncertainty is presented in Figure S9.

most significant during periods when the mixed layer is deep and vertical mixing rate is large, suggesting that this may be associated with vertical fluxes. However, the mixed layer budget also neglects some production in the middle part of the year when the mixed layer is shallower than the euphotic depth. Furthermore, without detailed measurements of the C:N ratio through time in all organic matter pools, we are unable to assess the effects of assuming constant ratios in DOM and POM. Using the Monte Carlo approach, we estimate the uncertainty in our ANCP estimates of POC to be approximately ±35–50% and of DOC to be approximately ±35–120% in the mixed layer and euphotic zone (Figure S9). This large range in uncertainty is the result of the relative magnitude of the physics terms in the box model when using a varying box size (mixed layer) versus a near-constant box size (euphotic zone), as well as the higher vertical transport rate at the base of the mixed layer. Nevertheless, these results suggest that this is a useful approach for distinguishing the relative composition of NCP into POC and DOC pools. However, the large amount of data collected via floats in this region helps reduce the uncertainty in our analysis, so the overall uncertainty would likely be larger if applied to parts of the ocean with less data coverage.

4.5. Comparison to Satellite-Derived Parameters

Figure 8 presents 8-day NPP estimates from the VGPM and CbPM satellite algorithms (top panel), as well as carbon export estimated using these NPP rates and the e-ratio algorithms of Laws et al. (2011) and Henson et al. (2011), extracted at the location of each of the floats from mid-2010 to early 2016. Note that the gaps in each time series during the winter months are due to cloud cover and/or high solar zenith angle. During this ~5-yr period, two floats (6400 and 7601) were equipped with optical sensors to measure particle backscatter (b_{bp}; Figure 2 timeline). The bottom panel of Figure 8 presents POC concentration estimated from the backscatter data set using the Graff et al. (2015) formulation ([POC] = (b_{bp}*48,811 − 24)/12). Note that during the year of 2012, the two floats overlapped in time, so a mean of the measurements was used in Figure 8.

Qualitatively, the highest annual POC concentration in the surface mixed layer occurred during the summer months and corresponded well with highest NPP and export rates estimated by satellite. Particle backscatter in the mesopelagic (~100–300 m) exhibits the seasonality of typically higher POC inventories in spring/summer than in fall/winter as well as large spring-bloom flux events during 2010 and 2015. These months-long events were only observed twice in the 6-yr-long record of particle backscatter, suggesting that they are atypical of any annual phenomenon. To quantify the annual pattern of particulate transfer with depth, we calculated a transfer efficiency from the surface mixed layer and euphotic zone to the 100- and 200-m horizons, respectively, by dividing the integrated POC concentration in 400-m depth zones (from 100 to 500 m and 200 to 600 m) by the integrated POC concentration in the mixed layer and euphotic zone (Figures 9c and 9d). When calculating the transfer efficiency, we apply a lag to account for the time it takes sinking particles to reach the deeper horizons. We account for sinking time between MLD or Z_{eu} and 100 or 200 m in our calculations by using the integrated concentration in the deeper depth zone calculated ~2 weeks (for 100 m) and 1 month (for 200 m) later than our mixed layer and euphotic zone NCP, respectively, which assumes a sinking velocity of ~5 m day^{-1}. One result of this approach is that the transfer efficiency between the mixed layer and 200 m is slightly larger than that of the mixed layer to 100 m at three time points in the climatology presented in Figure 9d (gray and black lines). The main advantage of this approach is that it does not rely on the

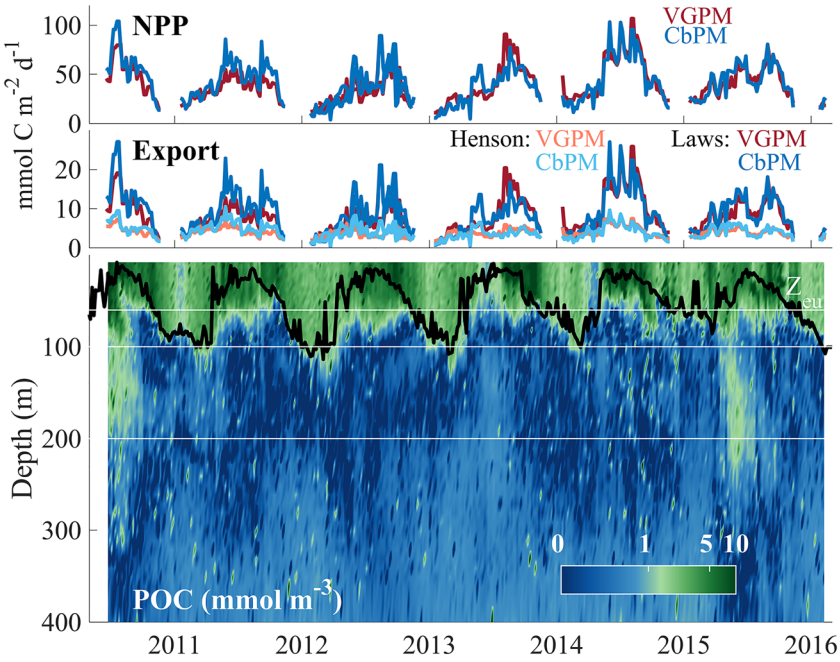

Figure 8. Net primary production calculated at the float locations using the VGPM and CbPM satellite algorithms (top panel) over the 5-yr period that floats collected optical sensor data. Carbon export calculated from the NPP estimates in the top panel and the algorithms of Henson et al. (2011) and Laws et al. (2011) (middle panel). Gaps are due to cloud cover in winter and/or high solar zenith angle. Water column POC concentration calculated using the formulation of Graff et al. (2015) (bottom panel; note that the colorbar is on a log scale) from particle backscatter measured by two floats, 6400 and 7601. The two floats overlapped for 2012, and so a mean of the measurements from each float was used during that year. White lines indicate the depth horizons used in the POC attenuation calculations: euphotic depth (Z_{eu}), 100 m, and 200 m.

absolute magnitude of POC concentration, but instead, it is independent of the choice of the b_{bp} to [POC] relationship because we use a ratio of POC inventories in the attenuation calculation. Of course, we cannot distinguish between sinking and suspended particles in the data set (see Figure 1), so the calculated transfer efficiencies are likely lower limits, but the uncertainty introduced through including the suspended portion is likely within our estimated uncertainty in our export estimates (~ ±50%).

As an alternative to budget-based NCP calculated deeper in the water column, which may be biased due to laterally advected signals in deeper water masses, we present POC export estimates across the 100- and 200-m horizons (Figure 9a) calculated as the transfer efficiencies presented in Figures 9c and 9d multiplied by the estimates of the POC portion of NCP in the mixed layer and euphotic zone presented in Figure 7. The gray and blue clouds represent the POC export to horizons of 100 and 200 m. We multiply the transfer efficiency by the POC NCP because at steady state, this is equivalent to POC exported out of the mixed layer and euphotic zone, respectively, and the transfer efficiency is an estimate of the attenuation of particles with depth to 100 and 200 m, respectively. This approach provides an in situ estimate of particle export, which tracer budgets in the mixed layer or euphotic zone alone are unable to achieve because they lack an estimate of particle attenuation with depth (i.e., the fraction of particles produced that do not escape the depth horizon of interest). We neglect any time periods where there was an estimated net heterotrophy in the mixed layer or euphotic zone for this analysis. We also plot carbon export estimates derived from satellite parameters extracted for the same time period averaged over our study region using the algorithms of Laws et al. (2011) in red and Henson et al. (2011) in orange on the same axes for comparison. Figure 9b shows the resulting export ratio from our calculated export rate divided by a climatological mean of the CbPM NPP data shown in the top panel of Figure 8, and those calculated using the Laws et al. (2011) and Henson et al. (2011) algorithms.

The only portion of the annual cycle of our e-ratio and export calculated from geochemical budgets and POC attenuation that agrees with both satellite algorithms between the 100- and 200-m horizons was from the

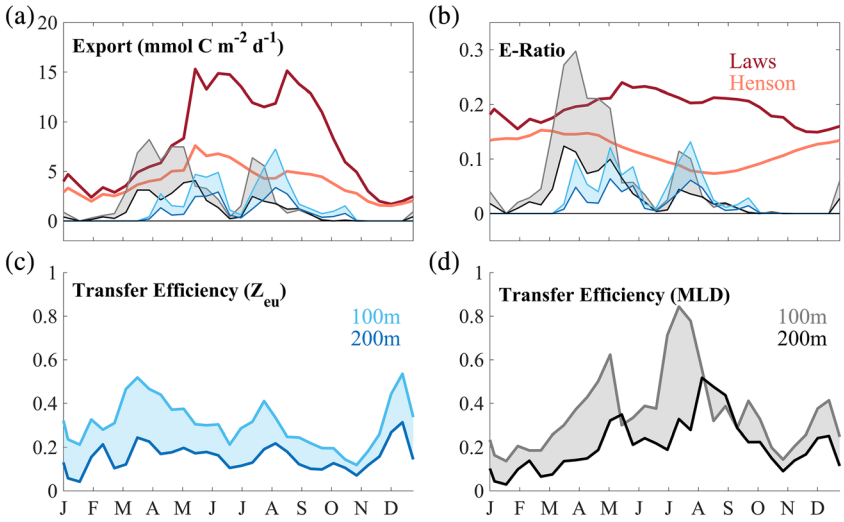

Figure 9. (a) Export of organic carbon across the 100-m (upper/lighter blue and gray lines) and 200-m horizons (lower/darker blue and gray lines) calculated by multiplying the climatological results of the mixed layer (gray) and euphotic zone (blue) tracer budget-calculated POC portion of NCP by the climatological mean transfer efficiency calculated from b_{bp}-calculated POC attenuation shown in (c) and (d). The clouds represent the region between 100 and 200 m. (b) Export ratio calculated as the export shown in (a) divided by CbPM NPP from the region (top panel in Figure 8). (c) Transfer efficiency from the euphotic depth to 100 m (light blue) and 200 m (dark blue) calculated as the attenuation of POC between these two horizons. (d) Transfer efficiency from the mixed layer depth to 100 m (light gray) and 200 m (black), respectively. For comparison, e-ratios from the Laws et al. (2011) and Henson et al. (2011) satellite export algorithms and export calculated from these algorithms using CbPM-calculated NPP (climatologies of data shown in middle panel in Figure 8) are presented as dark red and orange lines in (a) and (b). The months of November and December are linearly interpolated for the satellite-derived terms due to cloud cover in winter.

mixed layer budget during the spring months (March–May). During the late summer (July–August), the Henson et al. (2011) algorithm agreed well with both the mixed layer and euphotic zone budget approaches, but the Laws et al. (2011) algorithm was much larger. For the rest of the annual cycle, both satellite-based approaches overestimate e-ratio and export when compared to the tracer budget and POC attenuation approach. Furthermore, the seasonality of our export estimates appears to be shifted earlier in the year than those of Laws et al. (2011) and Henson et al. (2011), and the seasonality of the e-ratio appears to agree more with the Laws et al. (2011) approach overall, albeit with a phase shift, whereas the Henson et al. (2011) approach aligns well with our e-ratio during the spring and summer months. Overall, the seasonality of the satellite-based algorithms does not align with that of our geochemical budget-based NCP or POC export, perhaps because of their reliance on the seasonal cycle of NPP. Previous studies have shown that seasonal cycles in carbon export do not necessarily reflect the seasonal cycle in primary production (Haskell et al., 2017).

The annually integrated export values show that the Henson et al. (2011) satellite-based estimates are approximately ~1.5 to 2 times larger than the best estimates using the tracer budget and attenuation approach for POC export at 100 m (right side of Table 2), but our estimates have a large associated uncertainty. Furthermore, the Henson et al. (2011) annual export estimate agrees within uncertainty of our DIC budget-based approach, and to within ±50% of our nitrate budget approach, when calculated using the entire upper 100 m of the water column (left side of Table 2). However, the NCP budget approaches include DOC production as well, whereas the Henson et al. (2011) algorithm was developed using only POC export estimates at 100 m derived from ^{234}Th budgets for validation. When compared to our budget-based decomposition of the POC production in the upper 100 m (column labeled "POC"), the Henson et al. (2011) algorithm is approximately 3 times larger than our estimate. The Laws et al. (2011) algorithm estimates represent a value between total (POC + DOC) export from the euphotic depth horizon (NCP) and POC export across a deeper horizon, and while it is ~3–6 times larger than our POC export estimates using the budget and attenuation approach at 100 and 200 m, it is only ~1.5 and ~2.5 times larger than our budget-based approaches of total NCP and POC NCP evaluated to the euphotic depth. Regardless of the

Table 2
Annual NCP and POC Export Estimates Across Various Horizons Derived From the Various Approaches Presented (all in mol C m^{-2} yr^{-1})

	Budgets			DIC budget + POC attenuation		Satellite	
Horizon	DIC	NO_3[a]	POC	MLD	Z_{eu}	Laws	Henson
MLD	2.1 ± 1.0	2.1 ± 1.0	1.6 ± 0.8	-	-	-	-
Z_{eu}	2.0 ± 0.6	1.7 ± 0.6	1.4 ± 0.5	-	-	2.9	-
100 m	1.7 ± 0.7	1.0 ± 0.4	0.5 ± 0.2	0.9 ± 0.5	0.8 ± 0.4	-	1.5
MaxMLD	1.4 ± 0.6	1.2 ± 0.5	−0.5 ± 0.2	-	-	-	-
200 m	-	-	-	0.4 ± 0.2	0.4 ± 0.2	-	-

Note. Uncertainties estimated using the Monte Carlo approach described in the text and the values in the POC column are derived from the DIC budget.
[a]Estimated using a C:N of 7.8, found by balancing MLD ANCP.

approach used for comparison, the results of this study suggest that the Laws et al. (2011) algorithm also overestimates POC export in our study region.

Previous studies that compare satellite algorithm-based export at OSP have found similar results. Emerson (2014) reported the Laws et al. (2000) algorithm, which is similar to the Laws et al. (2011) algorithm used here, estimated e-ratios of 0.18–0.49 (mean 0.31) throughout the annual cycle and a total carbon export out of the euphotic zone (NCP) of 3.2 ± 0.6 to 4.5 ± 0.5 mol C m^{-2} yr^{-1} depending on the use of CbPM or VGPM NPP, which were both larger than geochemical estimates of 2.3 ± 0.6 mol C m^{-2} yr^{-1}. Palevsky et al. (2016) also used the Laws et al. (2000) algorithm in concert with CbPM-based NPP to calculate an ANCP of 3.2 ± 0.7 mol C m^{-2} yr^{-1} from 2003 to 2013 at OSP but noted that the fortuitous combination of underestimated NPP from the CbPM model and overestimated e-ratio is what makes this estimate fall into the range of uncertainty of the geochemical estimates. These authors add that the combination of VGPM NPP and Henson et al. (2011) recreated geochemistry-based ANCP best at OSP, but seasonality at this location was not discussed.

For comparison, Wong et al. (2002) and Peña and Varela (2007) determined ANCP rates at OSP of 1.5 ± 0.4 and 1.6 ± 0.6 mol C m^{-2} yr^{-1}, respectively, by seasonal nitrate drawdown in the upper 35 m from measurements made on Line P cruises spanning over 30 yr. Charette et al. (1999) determined euphotic zone POC export to be approximately 2.0 ± 1.0 mol C m^{-2} yr^{-1} based on ^{234}Th budgets and POC:^{234}Th measured on filtered particles. Other geochemical-based budgets using measurements of oxygen and nitrate summarized by Emerson (2014) indicate a mean ANCP of 2.3 ± 0.6 mol C m^{-2} yr^{-1}. All of these estimates are in agreement with our euphotic zone budgets of DIC and nitrate within uncertainty of the approaches. To our knowledge, the shallowest published sediment trap data at Station Papa are from 200 m from 1989 to 2006 (Timothy et al., 2013; Wong et al., 1999). Wong et al. (1999) reported an annual POC export of 0.55 ± 0.22 mol m^{-2} yr^{-1} at this depth horizon, and after this time series was continued through 2006, Timothy et al. (2013) reported an annual POC export rate of 0.46 ± 0.32 mol m^{-2} yr^{-1} at 200 m. These POC export rates agree well with our estimates at 200 m, which converge to 0.4 ± 0.2 mol m^{-2} yr^{-1} using both the mixed layer and euphotic zone budgets (Table 2). Overall, our POC attenuation approach provides a new method to estimate in situ POC export from surface geochemical budgets across a range of depth horizons using a combination of chemical and bio-optical sensor measurements on autonomous sampling platforms.

5. Discussion and Conclusions

In this study, we use observations of chemical and optical properties measured by autonomous BGC profiling floats over the last decade, as well as carbonate system parameters calculated from recently developed algorithms, to calculate NCP, an analog of carbon export out of the surface ocean. We chose to make these calculations for multiple depth zones (Figure 5), in part, to demonstrate the importance of this choice. Many carbon export studies neglect to address the implications for using a constant depth horizon in their estimates of the sink for atmospheric carbon dioxide. Evaluating the amount of carbon export that is available to be sequestered in the deep sea would mean that even if it is remineralized back to inorganic carbon, it still escapes ventilation when the seasonal winter MLD reaches its maximum (Palevsky & Doney, 2018; Palevsky & Quay, 2017). For example, export across the euphotic depth in spring, just after seasonal mixed layer shoaling, is likely to have enough time to sink past the local maximum MLD by winter when deep

mixing occurs, whereas after the summer months, only export across the maximum MLD is likely to escape re-entrainment and thus be separated from the atmosphere over long timescales. Furthermore, particle sinking speeds likely vary through time as particles are deteriorated by heterotrophic organisms along their journey to the deep. Because of this, our biweekly and annual NCP rate estimates (each point in Figure 5) across any single horizon are likely insufficient to estimate actual annual carbon sequestration. Using a time-variable depth horizon tuned for each individual annual cycle may further improve the quantification of true particle export, which is beyond the scope of this project.

We then use estimates of the C:N ratio of POM and DOM in our study region to further partition NCP into net production of POC and DOC in our budgets (Figure 7). Our estimate of the mean POC:DOC ratio in NCP is similar to the commonly reported value of ~70/30, and our net DOC production rates are similar to previously published estimates at our study site during the same time period (Bif & Hansell, 2019). As often observed in this region, we found net heterotrophy in the surface ocean during the winter months, and while our results suggest that a portion of this negative NCP is supported by POC, the majority is supported by the DOC pool, which has been hypothesized as an explanation for concurrent net heterotrophy and sinking particle export (Fassbender et al., 2016). Net calcium carbonate production was observed in late spring in the mixed layer and euphotic zone budgets, coinciding with the spring bloom, and in the euphotic zone budget, there is a second calcite production period in early fall.

In order to estimate particulate carbon export across deeper horizons (100 and 200 m) aided by information gathered by particle backscatter measurements (Figure 8), we calculate a transfer efficiency of sinking particles using optical measurements from the base of the mixed layer and euphotic zone to these deeper horizons and then multiplied these values by the budget-calculated NCP of POC in the mixed layer and euphotic zone (Figure 9). These POC export estimates agree well with our budget-calculated results to 100 m and previously published sediment trap export rates at 200 m (Table 2). However, concurrent satellite-derived carbon export estimates do not accurately capture the seasonal cycle and are typically significantly larger in magnitude than the in situ data through the year, indicating that they may overestimate carbon export in this region.

The largest contributor to uncertainty when using any biogeochemical budget approach to estimate biological production rates is typically the constraint on physical dynamics in the model (Haskell & Fleming, 2018; Teeter et al., 2018). We intentionally chose a region of the ocean where we could reliably parameterize the transport terms to test this new approach in deconstructing NCP into POC and DOC pools, and we urge that careful consideration of possible physical biases to the biological signal be given by researchers applying this method in more dynamic regions of the ocean. Furthermore, this work describes a carefully applied approach to a specific region of the ocean with available concurrent and historical measurements to leverage. While broad-scale application of this method to BGC floats could improve our understanding of upper ocean carbon cycling, more work is needed to test and improve methodology robustness in other domains.

As new, "fully loaded" BGC Argo floats (NO_3^-, O_2, pH, and bio-optical sensors; Johnson et al., 2017) are used more widely in the oceanographic community, the approaches described in this work could be applied with less reliance on carbonate system algorithms and further our understanding of the patterns of global carbon export to the deep. The relative partitioning of NCP into sinking particles and downward mixing of DOM, as well as the production/dissolution of the ballast material $CaCO_3$, has significant implications regarding the efficiency with which our ocean biosphere can sequester carbon originally sourced from the atmosphere (Bach et al., 2016; Hansell et al., 2009; Henson et al., 2019). This work represents a step toward a robust approach to estimate POC and DOC production and export in the oceans using autonomous, in situ observations for monitoring future changes in the ocean carbon cycle in near real-time. We have also shown the utility of relating in situ, autonomous biogeochemical observations to satellite-retrievable parameters, which we hope will be applied in efforts to improve satellite-based remote observations of ocean biogeochemistry.

Data Availability Statement

All data presented here are archived and can be accessed from MBARI FloatViz (https://www.mbari.org/science/upper-ocean-systems/chemical-sensor-group/floatviz/) or Station Papa website (http://www.water-properties.ca/linep).

Acknowledgments

Thanks to the captain and crew of the CCGS *John P. Tully* and the Line P program of the Institute of Ocean Sciences, Department of Oceans and Fisheries Canada, Sophia Johannessen, Cindy Wright, and Chelsi Lopez for assistance in collecting the data for calibration and validation of our sensor-based measurements. We would like to thank Ken Johnson for lending his expertise and guidance to the analysis of float-based data sets. Special thanks to Mariana Bif, Dennis Hansell, Craig Carlson, and Brandon Stephens for providing estimates of DOM nutrient ratios in the North Pacific and thoughtful insight on the topic. Support for this work was provided by a grant from the Chemical Oceanography program of the National Science Foundation to A. Fassbender (OCE1334398) and the David and Lucile Packard Foundation.

References

Anderson, L. A., & Sarmiento, J. L. (1994). Redfield ratios of remineralization determined by nutrient data analysis. *Global Biogeochemical Cycles*, *8*(1), 65–80. https://doi.org/10.1029/93gb03318

Armstrong, R. A., Lee, C., Hedges, J. I., Honjo, S., & Wakeham, S. G. (2002). A new, mechanistic model for organic carbon fluxes in the ocean based on the quantitative association of POPC with ballast minerals. *Deep Sea Research Part II: Topical Studies in Oceanography*, *49*, 219–236. https://doi.org/10.1016/s0967-0645(01)00101-1

Ayers, J. M., & Lozier, M. S. (2012). Unraveling dynamical controls on the North Pacific carbon sink. *Journal of Geophysical Research*, *117*, C01017. https://doi.org/10.1029/2011JC007368

Bach, L. T., Boxhammer, T., Larsen, A., Hildebrandt, N., Schulz, K. G., & Riebesell, U. (2016). Influence of plankton community structure on the sinking velocity of marine aggregates. *Global Biogeochemical Cycles*, *30*, 1145–1165. https://doi.org/10.1002/2016GB005372

Behrenfeld, M. J., & Falkowski, P. G. (1997). Photosynthetic rates derived from satellite-based chlorophyll concentration. *Limnology and Oceanography*, *42*(1), 1–20. https://doi.org/10.4319/lo.1997.42.1.0001

Bif, M. B., & Hansell, D. A. (2019). Seasonality of dissolved organic carbon in the upper Northeast Pacific Ocean. *Global Biogeochemical Cycles*, *33*, 526–539. https://doi.org/10.1029/2018gb006152

Bittig, H. C., & Körtzinger, A. (2015). Tackling oxygen optode drift: Near-surface and in-air oxygen optode measurements on a float provide an accurate in-situ reference. *Journal of Atmospheric and Oceanic Technology*, *32*(8), 1536–1543. https://doi.org/10.1175/JTECH-D-14-00162.1

Bittig, H. C., Steinhoff, T., Claustre, H., Fiedler, B., Williams, N. L., Sauzède, R., et al. (2018). An alternative to static climatologies: Robust estimation of open ocean CO_2 variables and nutrient concentrations from T, S, and O_2 data using Bayesian neural networks. *Frontiers in Marine Science*, *5*, 1–29. https://doi.org/10.3389/fmars.2018.00328

Boyd, P. W., Claustre, H., Levy, M., Siegel, D. A., & Weber, T. (2019). Multi-faceted particle pumps drive carbon sequestration in the ocean. *Nature*, *568*(7752), 327–335. https://doi.org/10.1038/s41586-019-1098-2

Brix, H., Gruber, N., Karl, D. M., & Bates, N. R. (2006). On the relationships between primary, net community, and export production in subtropical gyres. *Deep Sea Research Part II: Topical Studies in Oceanography*, *53*(5–7), 698–717. https://doi.org/10.1016/j.dsr2.2006.01.024

Broecker, W. S., & Peng, T.-H. (1974). Gas exchange rates between air and sea. *Tellus*, *26*(1–2), 21–35. https://doi.org/10.1111/j.2153-3490.1974.tb01948.x

Bushinsky, S. M., & Emerson, S. (2015). Marine biological production from in situ oxygen measurements on a profiling float in the subarctic Pacific Ocean. *Global Biogeochemical Cycles*, *29*, 2050–2060. https://doi.org/10.1002/2015GB005251

Bushinsky, S. M., & Emerson, S. R. (2018). Biological and physical controls on the oxygen cycle in the Kuroshio Extension from an array of profiling floats. *Deep Sea Research Part I: Oceanographic Research Papers*, *141*, 51–70. https://doi.org/10.1016/j.dsr.2018.09.005

Carlson, C. A., Ducklow, H. W., & Michaels, A. F. (1994). Annual flux of dissolved organic carbon from the euphotic zone of the northwest Sargasso Sea. *Nature*, *371*(6496), 405–408. https://doi.org/10.1038/371405a0

Carter, B. R., Feely, R. A., Williams, N. L., Dickson, A. G., Fong, M. B., & Takeshita, Y. (2017). Updated methods for global locally interpolated estimation of alkalinity, pH, and nitrate. *Limnology and Oceanography: Methods*, *16*(2), 119–131. https://doi.org/10.1002/lom3.10232

Charette, M. A., Moran, S. B., & Bishop, J. K. (1999). ^{234}Th as a tracer of particulate organic carbon export in the subarctic northeast Pacific Ocean. *Deep Sea Research Part II: Topical Studies in Oceanography*, *46*(11), 2833–2861. https://doi.org/10.1016/s0967-0645(99)00085-5

Cronin, M. F., Pelland, N. A., Emerson, S. R., & Crawford, W. R. (2015). Estimating diffusivity from the mixed layer heat and salt balances in the North Pacific. *Journal of Geophysical Research: Oceans*, *120*, 7346–7362. https://doi.org/10.1002/2015JC011010

Dall'Olmo, G., Dingle, J., Polimene, L., Brewin, R. J. W., & Claustre, H. (2016). Substantial energy input to the mesopelagic ecosystem from the seasonal mixed-layer pump. *Nature Geoscience*, *9*(11), 820–823. https://doi.org/10.1038/ngeo2818

de Boyer Montégut, C., Madec, G., Fischer, A. S., Lazar, A., & Iudicone, D. (2004). Mixed layer depth over the global ocean: An examination of profile data and a profile-based climatology. *Journal of Geophysical Research*, *109*, C12003. https://doi.org/10.1029/2004JC002378

De La Rocha, C. L., & Passow, U. (2014). 8.4—The biological pump. In H. D. H. K. Turekian (Ed.), *Treatise on geochemistry* (2nd ed., p. 1). Oxford: Elsevier.

del Giorgio, P. A., & Duarte, C. M. (2002). Respiration in the ocean. *Nature*, *420*(6914), 379–384. https://doi.org/10.1038/nature01165

Dickson, A. G. (1990). Standard potential of the reaction: AgCl(s) + 1/2H2(g) = Ag(s) + HCl (aq), and the standard acidity constant of the ion HSO4 in synthetic sea water from 273.15 to 318.15 K. *The Journal of Chemical Thermodynamics*, *22*(2), 113–127. https://doi.org/10.1016/0021-9614(90)90074-Z

Dunne, J. P., Armstrong, R. A., Gnanadesikan, A., & Sarmiento, J. L. (2005). Empirical and mechanistic models for the particle export ratio. *Global Biogeochemical Cycles*, *19*, GB4026. https://doi.org/10.1029/2004GB002390

Emerson, S. (1987). Seasonal oxygen cycles and biological new production in surface waters of the subarctic Pacific Ocean. *Journal of Geophysical Research*, *92*(C6), 6535–6544. https://doi.org/10.1029/JC092iC06p06535

Emerson, S. (2014). Annual net community production and the biological carbon flux in the ocean. *Global Biogeochemical Cycles*, *28*, 14–28. https://doi.org/10.1002/2013GB004680

Emerson, S., & Stump, C. (2010). Net biological oxygen production in the ocean—II: Remote in situ measurements of O_2 and N_2 in subarctic pacific surface waters. *Deep Sea Research Part I: Oceanographic Research Papers*, *57*(10), 1255–1265. https://doi.org/10.1016/j.dsr.2010.06.001

Emerson, S., Stump, C., & Nicholson, D. (2008). Net biological oxygen production in the ocean: Remote in situ measurements of O_2 and N_2 in surface waters. *Global Biogeochemical Cycles*, *22*, GB3023. https://doi.org/10.1029/2007GB003095

Emerson, S., Yang, B., White, M., & Cronin, M. (2019). Air-sea gas transfer: Determining bubble fluxes with in situ N_2 observations. *Journal of Geophysical Research: Oceans*, *124*, 2716–2727. https://doi.org/10.1029/2018jc014786

Fassbender, A. J., Sabine, C. L., & Cronin, M. F. (2016). Net community production and calcification from 7 years of NOAA Station Papa Mooring measurements. *Global Biogeochemical Cycles*, *30*, 250–267. https://doi.org/10.1002/2015GB005205

Garcia, H. E., Locamini, R. A., Boyer, T. P., Antonov, J. I., Zweng, M. M., Baranova, O. K., & Johnson, D. R. (2010). In S. Levitus (Ed.), *World Ocean Atlas 2009, Volume 4: Nutrients (phosphate, nitrate, silicate), NOAA Atlas NESDIS 71* (pp. 1–398). Washington, DC: US Government Publishing Office.

Graff, J. R., Westberry, T. K., Milligan, A. J., Brown, M. B., Dall'Olmo, G., van Dongen-Vogels, V., et al. (2015). Analytical phytoplankton carbon measurements spanning diverse ecosystems. *Deep Sea Research Part I: Oceanographic Research Papers*, *102*, 16–25. https://doi.org/10.1016/j.dsr.2015.04.006

Hansell, D. A., & Carlson, C. A. (2001). Biogeochemistry of total organic carbon and nitrogen in the Sargasso Sea: Control by convective overturn. *Deep Sea Research Part II: Topical Studies in Oceanography*, *48*(8–9), 1649–1667. https://doi.org/10.1016/s0967-0645(00)00153-3

Hansell, D. A., Carlson, C. A., Repeta, D. J., & Schlitzer, R. (2009). Dissolved organic matter in the ocean: A controversy stimulates new insights. *Oceanography*, *22*(4), 202–211. https://doi.org/10.5670/oceanog.2009.109

Haskell, W. Z. I. I., & Fleming, J. C. (2018). Concurrent estimates of carbon export reveal physical biases in ΔO_2/Ar-based net community production estimates in the Southern California Bight. *Journal of Marine Systems*, *183*, 23–31. https://doi.org/10.1016/j.jmarsys.2018.03.008

Haskell, W. Z. I. I., Prokopenko, M. G., Hammond, D. E., Stanley, R. H. R., & Sandwith, Z. O. (2017). Annual cyclicity in export efficiency in the inner Southern California Bight. *Global Biogeochemical Cycles*, *31*, 357–376. https://doi.org/10.1002/2016gb005561

Hennon, T. D., Riser, S. C., & Mecking, S. (2016). Profiling float-based observations of net respiration beneath the mixed layer. *Global Biogeochemical Cycles*, *30*, 920–932. https://doi.org/10.1002/2016GB005380

Henson, S. A., Le Moigne, F., & Giering, S. (2019). Drivers of carbon export efficiency in the global ocean. *Global Biogeochemical Cycles*, *33*, 891–903. https://doi.org/10.1029/2018GB006158

Henson, S. A., Sanders, R., Madsen, E., Morris, P. J., Le Moigne, F., & Quartly, G. D. (2011). A reduced estimate of the strength of the ocean's biological carbon pump. *Geophysical Research Letters*, *38*, L04606. https://doi.org/10.1029/2011GL046735

Holte, J., & Talley, L. (2009). A new algorithm for finding mixed layer depths with applications to Argo data and Subantarctic Mode Water formation. *Journal of Atmospheric and Oceanic Technology*, *26*(9), 1920–1939. https://doi.org/10.1175/2009JTECHO543.1

Hsu, S., Meindl, E. A., & Gilhousen, D. B. (1994). Determining the power-law wind-profile exponent under near-neutral stability conditions at sea. *Journal of Applied Meteorology*, *33*(6), 757–765. https://doi.org/10.1175/1520-0450(1994)033%3c0757:DTPLWP%3e2.0.CO;2

Izett, R. W., Manning, C. C., Hamme, R. C., & Tortell, P. D. (2018). Refined estimates of net community production in the subarctic Northeast Pacific derived from ΔO_2/Ar measurements with N_2O-based corrections for vertical mixing. *Global Biogeochemical Cycles*, *32*, 326–350. https://doi.org/10.1002/2017GB005792

Johnson, K. S., Coletti, L. J., Jannasch, H. W., & Sakamoto, C. M. (2013). Long-term nitrate measurements in the ocean using the in situ ultraviolet spectrophotometer: Sensor integration into the APEX profiling float. *Journal of Atmospheric and Oceanic Technology*, *30*(8), 1854–1866. https://doi.org/10.1175/JTECH-D-12-00221.1

Johnson, K. S., Plant, J. N., Coletti, L. J., Jannasch, H. W., Sakamoto, C. M., Riser, S. C., et al. (2017). Biogeochemical sensor performance in the SOCCOM profiling float array. *Journal of Geophysical Research: Oceans*, *122*, 6416–6436. https://doi.org/10.1002/2017JC012838

Johnson, K. S., Plant, J. N., Riser, S. C., & Gilbert, D. (2015). Air oxygen calibration of oxygen optodes on a profiling float array. *Journal of Atmospheric and Oceanic Technology*, *32*(11), 2160–2172. https://doi.org/10.1175/JTECH-D-15-0101.1

Johnson, K. S., Riser, S. C., & Karl, D. M. (2010). Nitrate supply from deep to near-surface waters of the North Pacific subtropical gyre. *Nature*, *465*(7301), 1062–1065. https://doi.org/10.1038/nature09170

Kalnay, E., Kanamitsu, M., Kistler, R., Collins, W., Deaven, D., Gandin, L., et al. (1996). The NCEP/NCAR 40-year reanalysis project. *Bulletin of the American Meteorological Society*, *77*(3), 437–471. https://doi.org/10.1175/1520-0477(1996)077%3c0437:TNYRP%3e2.0.CO;2

Laws, E. A., D'Sa, E., & Naik, P. (2011). Simple equations to estimate ratios of new or export production to total production from satellite-derived estimates of sea surface temperature and primary production. *Limnology and Oceanography: Methods*, *9*, 593–601. https://doi.org/10.4319/lom.2011.9.593

Laws, E. A., Falkowski, P. G., Smith, W. O. Jr., Ducklow, H., & McCarthy, J. J. (2000). Temperature effects on export production in the open ocean. *Global Biogeochemical Cycles*, *14*(4), 1231–1246. https://doi.org/10.1029/1999GB001229

Letscher, R. T., Moore, J. K., Teng, Y.-C., & Primeau, F. (2015). Variable C : N : P stoichiometry of dissolved organic matter cycling in the Community Earth System Model. *Biogeosciences*, *12*(1), 209–221. https://doi.org/10.5194/bg-12-209-2015

Llort, J., Langlais, C., Matear, R., Moreau, S., Lenton, A., & Strutton, P. G. (2018). Evaluating Southern Ocean carbon eddy-pump from biogeochemical-Argo floats. *Journal of Geophysical Research: Oceans*, *123*, 971–984. https://doi.org/10.1002/2017JC012861

Lomas, M. W., & Bates, N. R. (2004). Potential controls on interannual partitioning of organic carbon during the winter/spring phytoplankton bloom at the Bermuda Atlantic time-series study (BATS) site. *Deep Sea Research*, *51*(11), 1619–1636. https://doi.org/10.1016/j.dsr.2004.06.007

Lorenzo, D., & Mantua, N. (2016). Multi-year persistence of the 2014/15 North Pacific marine heatwave. *Nature Climate Change*, *6*(11), 1042–1047. https://doi.org/10.1038/nclimate3082

Lueker, T. J., Dickson, A. G., & Keeling, C. D. (2000). Ocean pCO_2 calculated from dissolved inorganic carbon, alkalinity, and equations for K_1 and K_2: Validation based on laboratory measurements of CO_2 in gas and seawater at equilibrium. *Marine Chemistry*, *70*(1–3), 105–119. https://doi.org/10.1016/S0304-4203(00)00022-0

Manning, C. C., & Nicholson, D. P. (2018). gas_toolbox v1.0.4: MATLAB code used in Manning et al. GTWS-7 proceedings. Github. %3chttps://github.com/dnicholson/gas_toolbox%3e Accessed on Sept. 13, 2018

Manning, C. C., Stanley, R. H. R., Nicholson, D. P., & Squibb, M. J. (2016). Quantifying air-sea gas exchange using noble gases in a coastal upwelling zone. *Journal of Physics Conference Series*. (In Proceedings of the 7th International Symposium on Gas Transfer at Water Surfaces). https://doi.org/10.1088/1755-1315/35/1/012017

Martin, J. H., & Fitzwater, S. E. (1988). Iron deficiency limits phytoplankton growth in the north-east Pacific subarctic. *Nature*, *331*(6154), 341–343. https://doi.org/10.1038/331341a0

Martin, J. H., Knauer, G. A., Karl, D. M., & Broenkow, W. W. (1987). Vertex: Carbon cycling in the northeast Pacific. *Deep Sea Research*, *34*(2), 267–285. https://doi.org/10.1016/0198-0149(87)90086-0

Millero, F. J. (2007). The marine inorganic carbon cycle. *Chemical Reviews*, *107*(2), 308–341. https://doi.org/10.1021/cr0503557

Nicholson, D., Emerson, S., & Eriksen, C. C. (2008). Net community production in the deep euphotic zone of the subtropical North Pacific gyre from glider surveys. *Limnology and Oceanography*, *53*(5part2), 2226–2236. https://doi.org/10.4319/lo.2008.53.5_part_2.2226

Omand, M. M., D'Asaro, E. A., Lee, C. M., Perry, M. J., Briggs, N., Cetinić, I., & Mahadevan, A. (2015). Eddy-driven subduction exports particulate organic carbon from the spring bloom. *Science*, *348*(6231), 222–225. https://doi.org/10.1126/science.1260062

Oregon State University (OSU) (2018). Ocean productivity. http://www.science.oregonstate.edu/ocean.productivity/%3e. Accessed: March 2018

Owens, S. A., Buesseler, K. O., Lamborg, C. H., Valdes, J., Lomas, M. W., Johnson, R. J., et al. (2013). A new time series of particle export from neutrally buoyant sediment traps at the Bermuda Atlantic Time-series Study site. *Deep Sea Research*, *72*, 34–47. https://doi.org/10.1016/j.dsr.2012.10.011

Palevsky, H. I., & Doney, S. C. (2018). How choice of depth horizon influences the estimated spatial patterns and global magnitude of ocean carbon export flux. *Geophysical Research Letters*, *45*, 4171–4179. https://doi.org/10.1029/2017GL076498

Palevsky, H. I., & Quay, P. D. (2017). Influence of biological carbon export on ocean carbon uptake over the annual cycle across the North Pacific Ocean. *Global Biogeochemical Cycles*, *31*, 81–95. https://doi.org/10.1002/2016gb005527

Palevsky, H. I., Quay, P. D., & Nicholson, D. P. (2016). Discrepant estimates of primary and export production from satellite algorithms, a biogeochemical model, and geochemical tracer measurements in the North Pacific Ocean. *Geophysical Research Letters*, *43*, 8645–8653. https://doi.org/10.1002/2016GL070226

Pelland, N. A., Eriksen, C. C., Emerson, S. R., & Cronin, M. F. (2018). Seaglider surveys at Ocean Station Papa: Oxygen kinematics and upper-ocean metabolism. *Journal of Geophysical Research: Oceans*, *123*, 6408–6427. https://doi.org/10.1029/2018jc014091

Peña, M. A., & Varela, D. E. (2007). Seasonal and interannual variability in phytoplankton and nutrient dynamics along Line P in the NE subarctic Pacific. *Progress in Oceanography*, *75*(2), 200–222. https://doi.org/10.1016/j.pocean.2007.08.009

Plant, J. N., Johnson, K. S., Sakamoto, C. M., Jannasch, H. W., Coletti, L. J., Riser, S. C., & Swift, D. D. (2016). Net community production at Ocean Station Papa observed with nitrate and oxygen sensors of profiling floats. *Global Biogeochemical Cycles*, *30*, 859–879. https://doi.org/10.1002/2015GB005349

Riser, S. C., & Johnson, K. S. (2008). Net production of oxygen in the subtropical ocean. *Nature*, *451*(7176), 323–325. https://doi.org/10.1038/nature06441

Sakamoto, C. M., Johnson, K. S., & Coletti, L. J. (2009). Improved algorithm for the computation of nitrate concentrations in seawater using an in situ ultraviolet spectrophotometer. *Limnology and Oceanography: Methods*, *7*, 132–143. https://doi.org/10.4319/lom.2009.7.132

Sarmiento, J. L., & Siegenthaler, U. (1992). In P. G. Falkowski & A. D. Woodhead (Eds.), *Primary productivity and biogeochemical cycles in the sea* (pp. 317–332). New York: Plenum.

Signorini, S. R., McClain, C. R., Christian, J. R., & Wong, C. S. (2001). Seasonal and interannual variability of phytoplankton, nutrients, TCO_2, pCO_2 and O_2 in the eastern subarctic Pacific (ocean weather station Papa). *Journal of Geophysical Research*, *106*(C12), 31,197–31,215. https://doi.org/10.1029/2000JC000343

Steinberg, D. K., Carlson, C. A., Bates, N. R., Goldthwait, S. A., Madin, L. P., & Michaels, A. F. (2000). Zooplankton vertical migration and the active transport of dissolved organic and inorganic carbon in the Sargasso Sea. *Deep-Sea Research*, *47*(1), 137–158. https://doi.org/10.1016/S0967-0637(99)00052-7

Sutton, A. J., Sabine, C. L., Dietrich, C., Jones, S., Musielewicz, S., Bott, R., & Osborne, J. (2012). High-resolution ocean and atmosphere pCO_2 time-series measurements from mooring Papa_145W_50N in the North Pacific Ocean from 2010-06-15 to 2015-06-15 (NCEI Accession 0100074). *NOAA National Centers for Environmental Information*. https://doi.org/10.3334/cdiac/otg.tsm_papa_145w_50n Accessed: Sept. 15, 2019

Takahashi, T., Sutherland, S. C., Wanninkhof, R., Sweeney, C., Feely, R. A., Chipman, D. W., et al. (2009). Climatological mean and decadal change in surface ocean pCO_2, and net sea-air CO_2 flux over the global oceans. *Deep Sea Research Part II: Topical Studies in Oceanography*, *56*(8–10), 554–577. https://doi.org/10.1016/j.dsr2.2008.12.009

Takeshita, Y., Martz, T. R., Johnson, K. S., Plant, J. N., Gilbert, D., Riser, S. C., et al. (2013). A climatology-based quality control procedure for profiling float oxygen data. *Journal of Geophysical Research: Oceans*, *118*, 5640–5650. https://doi.org/10.1002/jgrc.20399

Teeter, L., Hamme, R. C., Ianson, D., & Bianucci, L. (2018). Accurate estimation of net community production from O2/Ar measurements. *Global Biogeochemical Cycles*, *32*, 1163–1181. https://doi.org/10.1029/2017gb005874

Tengberg, A., Hovdenes, J., Andersson, H. J., Brocandel, O., Diaz, R., Hebert, D., et al. (2006). Evaluation of a lifetime-based optode to measure oxygen in aquatic systems. *Limnology and Oceanography: Methods*, *4*(2), 7–17. https://doi.org/10.4319/lom.2006.4.7

Timothy, D. A., Wong, C. S., Barwell-Clarke, J. E., Page, J. S., White, L. A., & Macdonald, R. W. (2013). Climatology of sediment flux and composition in the subarctic Northeast Pacific Ocean with biogeochemical implications. *Progress in Oceanography*, *116*, 95–129. https://doi.org/10.1016/j.pocean.2013.06.017

Uppström, L. R. (1974). The boron/chlorinity ratio of deep-sea water from the Pacific Ocean. *Deep Sea Research*, *21*(2), 161–162. https://doi.org/10.1016/0011-7471(74)90074-6

van Heuven, S., Pierrot, D., Rae, J. W. B., Lewis, E., & Wallace, D. W. R. (2011). *MATLAB program developed for CO_2 system calculations ORNL/CDIAC-105b*. Oak Ridge, Tennessee: Carbon Dioxide Information Analysis Center, Oak Ridge Natl. Lab. U.S. Dep. Energy. https://doi.org/10.3334/CDIAC/otg.CO2SYS_MATLAB_v1.1

Volk, T., & Hoffert, M. I. (1985). Ocean carbon pumps: Analysis of relative strengths and efficiencies in ocean-driven atmospheric CO_2 changes. In E. T. Sundquist & W. S. Broecker (Eds.), *The carbon cycle and atmospheric CO_2: Natural variations Archean to present*, *Geophysical Monograph* (Vol. 32, pp. 99–110). Washington, DC: American Geophysical Union.

Wanninkhof, R. (1992). Relationship between wind speed and gas exchange over the ocean. *Journal of Geophysical Research*, *97*(C5), 7373–7382. https://doi.org/10.1029/92JC00188

Wanninkhof, R. (2014). Relationship between wind speed and gas exchange over the ocean revisited. *Limnology and Oceanography: Methods*, *12*(6), 351–362. https://doi.org/10.4319/lom.2014.12.351

Weiss, R. (1974). Carbon dioxide in water and seawater: The solubility of a non-ideal gas. *Marine Chemistry*, *2*(3), 203–215. https://doi.org/10.1016/0304-4203(74)90015-2

Westberry, T., Behrenfeld, M. J., Siegel, D. A., & Boss, E. (2008). Carbon-based primary productivity modeling with vertically resolved photoacclimation. *Global Biogeochemical Cycles*, *22*, GB2024. https://doi.org/10.1029/2007GB003078

Williams, N. L., Juranek, L. W., Feely, R. A., Russell, J. L., Johnson, K. S., & Hales, B. (2018). Assessment of the carbonate chemistry seasonal cycles in the Southern Ocean from persistent observational platforms. *Journal of Geophysical Research: Oceans*, *123*, 4833–4852. https://doi.org/10.1029/2017JC012917

Wolf-Gladrow, D., Zeebe, R. E., Klaas, C., Kortzinger, A., & Dickson, A. G. (2007). Total alkalinity: The explicit conservative expression and its application to biogeochemical processes. *Marine Chemistry*, *106*(1–2), 287–300. https://doi.org/10.1016/j.marchem.2007.01.006

Wong, C. S., Waser, N. A. D., Whitney, F. A., Johnson, W. K., & Page, J. S. (2002). Time-series study of the biogeochemistry of the North East subarctic Pacific: Reconciliation of the Corg/N remineralization and uptake ratios with the Redfield ratios. *Deep Sea Research Part II: Topical Studies in Oceanography*, *49*(24), 5717–5738. https://doi.org/10.1016/s0967-0645(02)00211-4

Wong, C. S., Whitney, F. A., Crawford, D. W., Iseki, K., Matear, R. J., Johnson, W. K., et al. (1999). Seasonal and interannual variability in particle fluxes of carbon, nitrogen and silicon from time series of sediment traps at Ocean Station P, 1982–1993: Relationship to changes in subarctic primary productivity. *Deep-Sea Research Part II*, *46*(11–12), 2735–2760. https://doi.org/10.1016/S0967-0645(99)00082-X

Yang, B., Emerson, S. R., & Bushinsky, S. M. (2017). Annual net community production in the subtropical Pacific Ocean from in situ oxygen measurements on profiling floats. *Global Biogeochemical Cycles*, *31*, 728–744. https://doi.org/10.1002/2016GB005545

Yang, B., Emerson, S. R., & Peña, M. A. (2018). The effect of the 2013–2016 high temperature anomaly in the subarctic Northeast Pacific (the "Blob") on net community production. *Biogeosciences*, *15*, 6747–6759. https://doi.org/10.5194/bg-15-6747-2018

Reference From the Supporting Information

Juranek, L. W., Feely, R. A., Gilbert, D., Freeland, H., & Miller, L. A. (2011). Real-time estimation of pH and aragonite saturation state from Argo profiling floats: Prospects for an autonomous carbon observing strategy. *Geophysical Research Letters*, *38*, L17603. https://doi.org/10.1029/2011GL048580